Experimental Hematology

Experimental Hematology 2015;43:1031–1046

FANCA safeguards interphase and mitosis during hematopoiesis in vivo

Zahi Abdul-Sater[a,b], Donna Cerabona[a,b], Elizabeth Sierra Potchanant[a], Zejin Sun[a], Rikki Enzor[a], Ying He[a], Kent Robertson[a], W. Scott Goebel[a], and Grzegorz Nalepa[a,b,c,d]

[a]*Herman B. Wells Center for Pediatric Research, Department of Pediatrics, Indiana University School of Medicine, Indianapolis, Indiana;* [b]*Department of Biochemistry and Molecular Biology, Indiana University School of Medicine, Indianapolis, Indiana;* [c]*Department of Medical and Molecular Genetics, Indiana University School of Medicine, Indianapolis, Indiana;* [d]*Bone Marrow Failure Program, Division of Pediatric Hematology–Oncology, Riley Hospital for Children, Indianapolis, Indiana*

(Received 18 August 2015; accepted 19 August 2015)

The Fanconi anemia (FA/BRCA) signaling network controls multiple genome-housekeeping checkpoints, from interphase DNA repair to mitosis. The in vivo role of abnormal cell division in FA remains unknown. Here, we quantified the origins of genomic instability in FA patients and mice in vivo and ex vivo. We found that both mitotic errors and interphase DNA damage significantly contribute to genomic instability during FA-deficient hematopoiesis and in non-hematopoietic human and murine FA primary cells. Super-resolution microscopy coupled with functional assays revealed that FANCA shuttles to the pericentriolar material to regulate spindle assembly at mitotic entry. Loss of FA signaling rendered cells hypersensitive to spindle chemotherapeutics and allowed escape from the chemotherapy-induced spindle assembly checkpoint. In support of these findings, direct comparison of DNA crosslinking and anti-mitotic chemotherapeutics in primary *FANCA−/−* cells revealed genomic instability originating through divergent cell cycle checkpoint aberrations. Our data indicate that FA/BRCA signaling functions as an in vivo gatekeeper of genomic integrity throughout interphase and mitosis, which may have implications for future targeted therapies in FA and FA-deficient cancers.

The Fanconi anemia (FA/BRCA) pathway is an intricate plexus of at least 17 proteins that maintain genomic stability, control growth and development, and prevent cancer. Bi-allelic germline disruption of any FA gene causes Fanconi anemia (FA), a genetic disorder characterized by developmental abnormalities, bone marrow failure (BMF), myelodysplasia, and high risk of cancer, particularly acute myeloid leukemia (AML) [1–5]. Heterozygous inborn mutations in the BRCA branch of the FA network increase risk of breast and ovarian cancers as well as other tumors [5–9], and somatic mutations of FA/BRCA genes occur in malignancies in non–Fanconi patients [10–13]. Thus, disruption of FA/BRCA signaling promotes malignancies in the inherited genetic syndromes and in the general population.

Offprint requests to: Grzegorz Nalepa, Herman B. Wells Center for Pediatric Research, Division of Pediatric Hematology–Oncology, Department of Pediatrics, Indiana University School of Medicine, 1044 West Walnut Street, R4-421, Indianapolis, IN 46202, USA; E-mail: gnalepa@iu.edu

Supplementary data related to this article can be found online at http://dx.doi.org/10.1016/j.exphem.2015.08.013.

The FA/BRCA pathway prevents cancer by protecting genome integrity. In interphase, the DNA damage response (DDR) initiates the assembly of the multiprotein FA complex at damage sites to arrest the cell cycle as the cascade of effectors repairs the lesions [1,5]. These compartmentalized bursts of FA activity handle multiple genotoxic insults, from endogenous aldehydes [14,15] to replication errors and mutagen exposure. Thus, the FA/BRCA network provides a crucial line of defense against interphase mutagenesis [1,5].

Less is known about the role of the FA/BRCA pathway during mitosis, but FA signaling has recently been implicated in the maintenance of normal centrosome count [16–19], spindle assembly checkpoint (SAC) [17,20], repair of anaphase bridges [21,22], and execution of cytokinesis [23–25]. Because chromosomal instability resulting from mitotic errors is a hallmark of cancer [26,27] and a therapeutic target [28], these findings may have translational relevance. However, it is unknown whether these ex vivo observations are applicable to in vivo hematopoiesis.

Here, we present quantitative evidence that loss of FA signaling disrupts mitosis during in vivo hematopoiesis in

http://dx.doi.org/10.1016/j.exphem.2015.08.013

humans and mice and that both aberrant interphase and mitotic failure contribute to genomic instability caused by FA deficiency. Super-resolution microscopy revealed that FANCA shuttles to the pericentriolar material at mitotic entry to regulate centrosome-associated spindle nucleation. We found that primary *FANCA−/−* cells escape chemotherapy-induced SAC to replicate despite genomic instability. Our cell survival assays indicated that FA-deficient cells are hypersensitive to taxol (an antimitotic chemotherapeutic agent). Sublethal taxol doses exacerbated genomic instability in FA−/− cells through mitotic errors, whereas low-dose mitomycin C (MMC) activated the G2/M checkpoint and DNA breakage. Therefore, distinct classes of chemotherapeutic agents inflict unique damage patters in FA−/− cells, which may have implications for future strategies against FA-deficient cancers. Together, our findings provide insights into complex mechanisms of genomic instability in FA.

Methods

Cell culture

The primary patient fibroblast cells, *FANCA−/−* (MNHN, RA885) and *FANCC−/−* (WD-C1, homozygous for FANCC$^{c.377_378delGA}$), were received from Dr. Helmut Hanenberg (Indiana University [IU]). MNHN cells harbor two *FANCA* mutations: c.3163C>T and c.4124-4125delCA. Both *FANCA*-deficient lines have been described and the functional gene correction of all cell lines used in this study has been validated in G2/M MMC hypersensitivity assays (Supplementary Figure E1, online only, available at www.exphem.org) [17]. Experiments were done using MNHN cells unless otherwise noted. Fibroblasts and mouse embryonic fibroblasts (MEFs) were cultured in Dulbecco's modified Eagle medium (DMEM) containing 10% fetal bovine serum (FBS), 1% penicillin–streptomycin (pen-strep), and 1% sodium pyruvate in 37°C 5% CO_2/5% O_2 incubators to minimize oxidative damage. Primary human CD34+ cells (IU Simon Cancer Center Angio BioCore) were incubated at 37°C in 5% CO_2/5% O_2 in Iscove's modified Dulbecco's medium (IMDM) with 20% FBS, 1% pen-strep, 100 ng/mL stem cell factor (SCF), 100 ng/mL thrombopoietin (TPO), and 100 ng/mL fms-like tyrosine kinase 3 (FLT3).

Mice

All animal experiments were approved by the Institutional Animal Care and Use Committee (IACUC) at IU School of Medicine. *Fancc−/−* mice [29] were a gift from Dr. D. Wade Clapp (IU).

RBC micronucleation assays

Fifty microliters of blood was collected from the murine lateral tail vein into EDTA-coated collection tubes containing methanol (2 mL, prechilled at −80°C for >1 hour) and stored in −80°C. Next, 10 mL phosphate-buffered saline (PBS) was added, and cells were pelleted at 600*g* (5 min, 4°C). The supernatant was aspirated, and red blood cells (RBCs) were resuspended in residual methanol/PBS. Twenty-microliter aliquots were transferred to flow tubes and incubated in the dark with 90 μL of fluorescein isothiocyanate (FITC)-conjugated anti-mouse CD71 (Biolegend) + 1 mg/mL RNase A (Roche), first for 30 min at room temperature (RT) and then for 30 min on ice. Propidium iodide (Invitrogen) staining at 1.25 μg/mL was followed by flow cytometry on a FacsCalibur machine (Becton-Dickinson). At least 500,000 events/sample were acquired. A Hemavet 950FS (Drew Scientific) was used for blood counts.

Deconvolution and super-resolution microscopy

Cells grown on ultrafine glass coverslips (Fisher) were fixed with 4% paraformaldehyde/PBS for 15 min (RT), PBS-washed, permeabilized with 0.1% Triton X-100/PBS for 10 min, PBS-washed, blocked in 5% bovine serum albumin (BSA)/PBS or ImageIT SignalEnhancer (Life Technologies) for 1 hour, and then incubated in primary antibody in 1% BSA/PBS overnight (4°C) or 2 hours (RT). Antibodies are listed in the Supplementary Methods (online only, available at www.exphem.org). Next, cells were PBS-washed and incubated with secondary antibodies (1:2,000, 1% BSA/PBS) for 30 min (RT), PBS-washed, counterstained with Hoechst-33342 (Life Technologies) in PBS (1:10,000) for 10 min, washed, and mounted in SlowFade Antifade (Life Technologies).

For deconvolution microscopy, image stacks (*z*-section distance: 0.2 μm) were acquired on a Deltavision PersonalDx microscope (Applied Precision) with a CCD camera using 20×, 60×, or 100× lenses and deconvolved using Softworx. Super-resolution structured illumination microscopy (SR-SIM) images were acquired on a Zeiss ELYRA PS.1 system with a CCD camera and 60×/100× lenses, and processed via SIM/channel-alignment algorithms (Zen-2011; Zeiss). Line-intensity profiles were quantified using Imaris (Bitplane). *z* Sections on figures were exported using Imaris.

Images of FA patient marrow aspirates, marrow aspirates of patients diagnosed with immune-mediated aplastic anemia with negative chromosome breakage test results, marrow cytospins, and peripheral smears were obtained on a Zeiss Axiolab microscope with Axiocam-105 color camera.

Cytokinesis-block micronucleus assays

Fibroblasts and MEFs grown on coverslips were treated with cytochalasin B (2 μg/mL) for 24 hours, followed by processing/imaging as described above; anti-CENPA immunofluorescence visualized endogenous kinetochores. For drug treatments, cells were exposed to 1 nmol/L taxol or MMC for 9 days before cytochalasin B for 24 hours. A micronucleus was defined based on the following criteria: (i) the diameter of the micronucleus must be less than half that of the main nucleus, and (ii) the nuclear boundary must be identified between the micronucleus and the nucleus. The presence of kinetochores was determined based on visualization of CENPA+ foci within the stack of *z* sections spanning the entire micronucleus.

For CD34+ experiments, primary human CD34+ cells transduced with green fluorescent protein (GFP)-tagged lentiviral shRNA constructs were cultured for 5 days, sorted on a SORPAria FACS system, attached to coverslips via cytospin (450 rpm, 7 min), and analyzed in immunofluorescence assays as described above.

Mitotic spindle assembly assay

Culture plates with live fibroblasts on coverslips were removed from the 37°C incubator to replace growth medium with prechilled medium and kept at 4°C (1 hour). Next, the cold medium was replaced with prewarmed medium (37°C), and cells were returned to 37°C (15 sec) and immediately fixed (4% paraformaldehyde/PBS). On

staining with anti-pericentrin and anti-α-tubulin, cells were imaged via deconvolution microscopy. Imaris (Bitplane) was used to measure length of microtubules in z sections and count centrosome-associated microtubules within stacks.

Statistics

Statistical analyses were performed using GraphPad Prism 6. A p value < 0.05 was considered to indicate significance.

Study approval

Patients had been enrolled on the institutional review board-approved protocol at IU School of Medicine (IRB No. 1108006474). All animal experiments were approved by the Institutional Animal Care and Use Committee (IACUC) at IU School of Medicine.

Results

In vivo error-prone mitosis during FA−/− hematopoiesis

Mitotic failure was reported in FA cells ex vivo, and cytokinesis failure was documented in FA marrows [17,23]. However, the in vivo evidence of abnormal early mitosis in hematopoietic cells of FA patients has been missing. To examine whether loss of *FANCA* (the gene most commonly disrupted in FA [5]) predisposes hematopoietic cells to erratic divisions in vivo, we quantified mitotic errors in marrow aspirates of two *FANCA−/−* patients with pancytopenia but no MDS/AML. Consistent with the role of FANCA in cell division, we observed an increased frequency of abnormal mitotic figures in *FANCA−/−* marrows compared with marrow aspirates of patients diagnosed with immune-mediated aplastic anemia after excluding FA by negative chromosome breakage tests ($p = 0.01$) (Fig. 1A). Lack of chromosome congression leading to lagging chromosomes in anaphase and micronucleation at mitotic exit reflects weakened SAC or merotelic attachment caused by centrosome malfunction [17]. The DNA bridges in late mitosis may reflect impaired resolution of ultrafine anaphase bridges [21]. Interphase nuclear morphology in the erythroid lineage provided further evidence of in vivo mitotic abnormalities (Fig. 1B, C). Erythroblast micronucleation (Fig. 1B) suggests failure to segregate chromosomes into the daughter nuclei. The presence of bizarre erythroblasts with multilobed nuclei (Fig. 1B) is consistent with impaired chromosome segregation caused by erroneous SAC followed by cytokinesis failure [17,23]. Binucleated erythroblasts (Fig. 1B) reflect lack of cytokinesis after normal chromosome division [23]. These results provide quantitative in vivo evidence that abnormal mitoses occur with increased frequency in the hematopoietic cells of *FANCA−/−* patients before development of MDS/AML.

We next validated these findings in a different in vivo experimental system. We examined hematopoietic chromosomal instability in living *Fancc−/−* mice using an in vivo erythrocyte micronucleation assay [30,31]. This assay is based on the notion that genomically unstable orthochromatic erythroblasts fail to extrude micronuclei, producing micronucleated RBCs. Indeed, we observed micronucleated RBCs in FA patients' marrows (Fig. 1C). These micronucleated RBCs are identified via flow cytometry as DNA-containing CD71– RBCs (Fig. 1D). Three-month old *Fancc−/−* mice released almost threefold more micronucleated mature RBCs into the peripheral blood than did age-matched controls ($p < 0.0001$) (Fig. 1D). Importantly, blood counts revealed no differences between the age-matched wild-type and *Fancc−/−* mice (Supplementary Table E1, online only, available at www.exphem.org). Thus, disruption of two different FA core genes (*FANCA* and *Fancc*) leads to chromosomal instability during in vivo hematopoiesis in humans and mice before the onset of clinically significant BMF, myelodysplasia or leukemia.

A combination of interphase and mitotic errors drives genomic instability in FA

As BMF and hematopoietic malignancies are consistent clinical hallmarks of FA [1,5], we quantified the contribution of interphase and mitotic abnormalities to genomic instability in FANCA-deficient hematopoietic cells. A modified micronucleus assay (Fig. 2A) [32] allowed us to determine the origin of multinucleation in primary human CD34+ hematopoietic cells transduced with an shRNA against *FANCA* [17], compared with control CD34+ cells. We validated the *FANCA* shRNA in human CD34+ cells (Fig. 2B, C). Upon FANCA knockdown, CD34+ cells were immunostained for endogenous CENPA (a kinetochore marker [33]) and imaged by deconvolution microscopy to classify cells based on the presence of CENPA+ foci. As described [32], additional kinetochore-positive nuclei arise through whole-chromosome missegregation in mitosis, and supernumerary kinetochore-negative nuclei result from DNA fragmentation (Fig. 2A). FANCA-knockdown CD34+ cells developed higher multinucleation because of both chromosome breakage ($p = 0.0083$) and faulty chromosome segregation ($p = 0.0001$), compared with control CD34+ cells (Fig. 2D, E). We concluded that silencing FANCA impairs both interphase and mitotic genome maintenance in human hematopoietic cells.

To validate this finding in primary FA-deficient patient cells and eliminate the possibility of nonspecific shRNA-induced phenotype [34], we pursued cytokinesis-block cytome assays [32]. Dividing cells are treated with cytochalasin B (a cytokinesis inhibitor) prior to CENPA immunofluorescence. Inhibition of cytokinesis generates binucleated cells on error-free chromosome partition, and the presence of micronuclei indicates abnormal chromosome segregation during the last mitosis. Again, CENPA positivity distinguishes mitotic-failure micronuclei from DNA-breakage micronuclei (Fig. 3A) [35].

FANCA−/− fibroblasts had an increased frequency of both chromosome missegregation ($p = 0.0391$) and

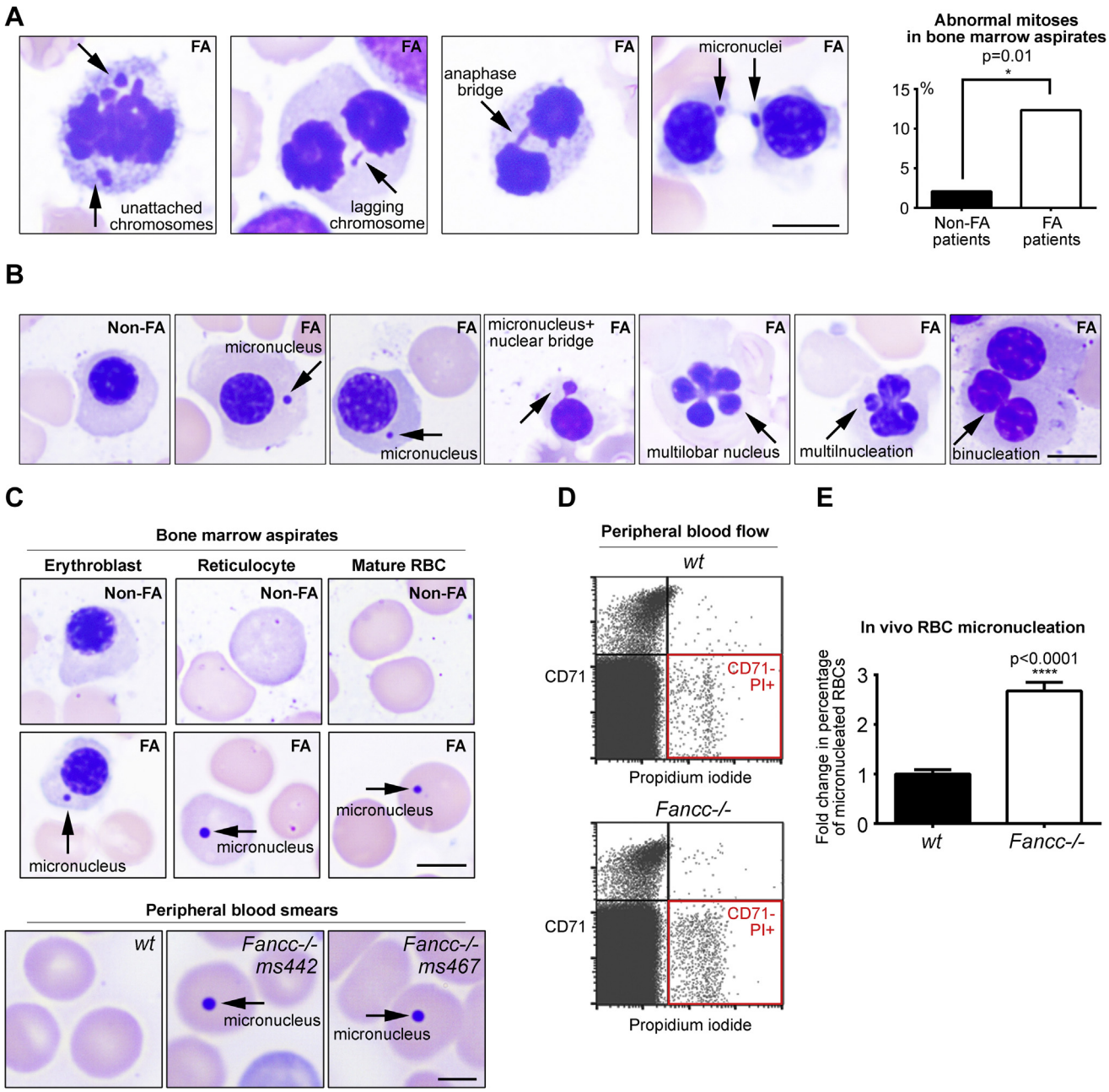

Figure 1. In vivo chromosomal instability and abnormal mitoses during human *FANCA–/–* and murine *Fancc–/–* hematopoiesis. **(A)** Representative abnormal mitoses in *FANCA–/–* patient bone marrow aspirates. Quantification (upper right) represents data from two different FA patients and two non-FA patients (96 mitoses in non-FA and 73 mitoses in FA; Fisher's exact test). Bar = 5 μm. **(B)** Examples of abnormal interphase nuclear morphology in *FANCA–/–* patients' hematopoietic cells that have undergone aberrant mitoses compared with a normal non-FA interphase erythroblast. Bar = 5 μm. **(C)** Micronucleation of *FANCA–/–* bone marrow erythroblasts, reticulocytes, and mature red blood cells (top) and *Fancc–/–* murine RBCs in peripheral blood (bottom). Bars = 5 μm (top) and 2 μm (bottom). **(D)** Increased frequency of CD71–, PI+ micronucleated mature RBCs in peripheral blood of 3-month-old *Fancc–/–* mice. **(E)** Quantification of micronucleated RBCs identified by flow cytometry is shown as fold change relative to wild-type levels. Bars indicate means ± SEM; >10 age-matched mice/genotype from multiple independent experiments were analyzed using Student's *t* test. All specimens were imaged with a Zeiss Axiolab system equipped with an Axiocam 105 color camera.

chromosome breakage ($p = 0.0218$) compared with isogenic gene-corrected cells (Fig. 3B, C). Similarly, *Fancc−/−* MEFs had an increased incidence of micronucleation resulting from both chromosome breakage ($p = 0.0004$) and chromosome missegregation ($p = 0.0078$) compared with wild-type MEFs (Fig. 3D, E). Thus, disruption of FA signaling impairs interphase and mitotic fidelity not only during hematopoiesis (Fig. 2), but also in fibroblasts and

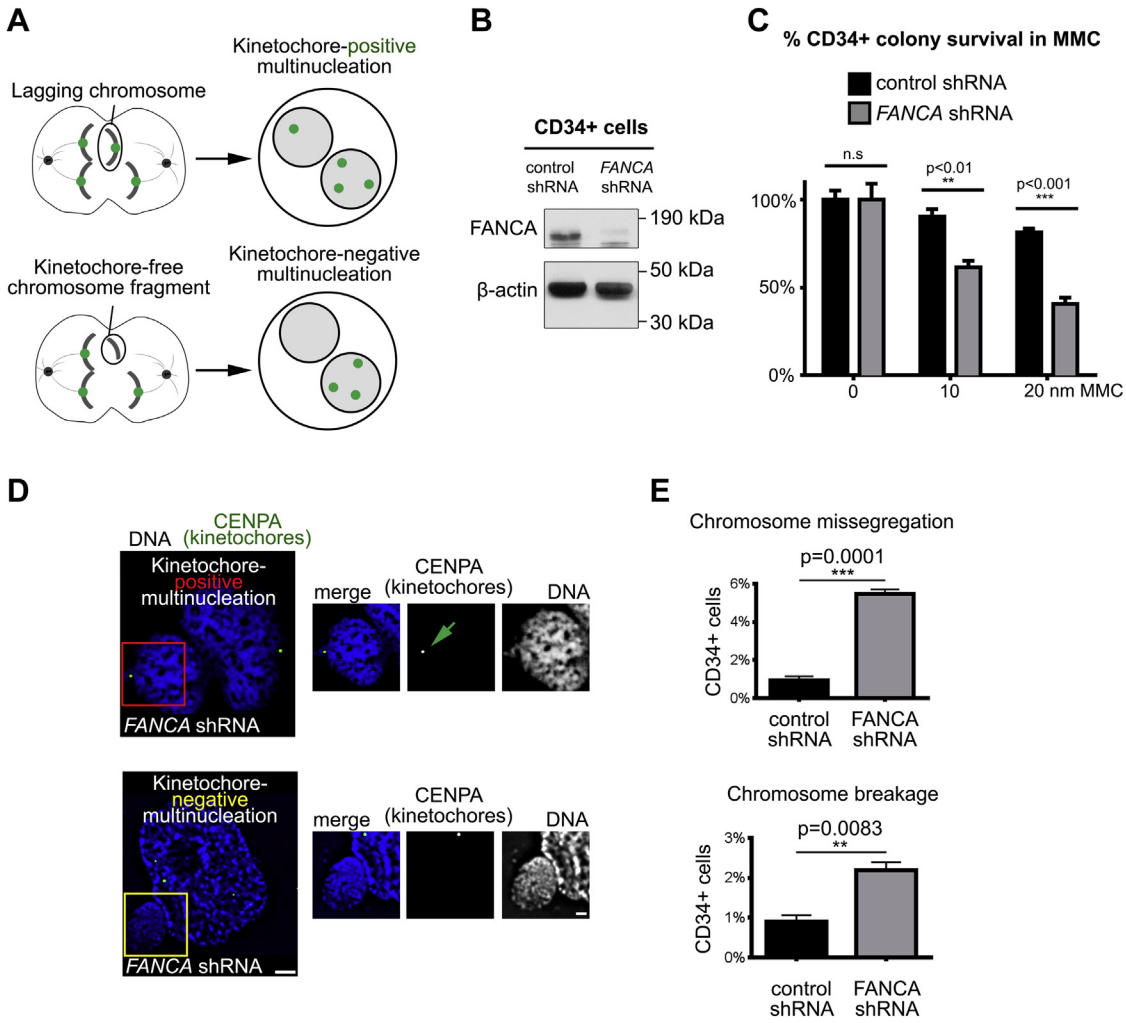

Figure 2. FANCA maintains genomic integrity during interphase and mitosis in primary human CD34+ cells. **(A)** Assay schematic. Kinetochore/centrosome immunofluorescence staining distinguishes multinucleation generated through whole-chromosome missegregation from multinucleation resulting from DNA breakage. **(B)** *FANCA* shRNA efficiently knocks down FANCA protein in primary human CD34+ cells. β-Actin serves as loading control. **(C)** Functional validation of *FANCA* shRNA in primary human CD34+ cells. *FANCA* shRNA renders CD34+ cells hypersensitive to mitomycin C as compared with CD34+ cells transduced with control shRNA. Error bars represent means ± SEM. Significance was determined using a two-way analysis of variance with Sidak correction. **(D)** Representative images of multinucleation resulting from FANCA knockdown in human CD34+ cells. Regions of interests are marked in *red* or *yellow* and enlarged on the right. *Green arrow* points to a CENPA-positive centromere/kinetochore within the supernumerary nucleus. Bars = 2 μm (left) and 1 μm (right) **(E)** Quantification of multinucleation resulting from weakened SAC or chromosome breakage in control and FANCA-knockdown CD34+ cells. At least 500 cells per group were counted. Results were analyzed using Student's *t* test and represented as means ± SEM.

MEFs (Fig. 3). These findings suggest that multiple FA/BRCA proteins may play evolutionarily conserved roles in mitotic genome housekeeping.

FANCA regulates centrosome-mediated spindle microtubule assembly in early mitosis

We and others have reported defects in centrosome amplification in cells lacking the FA/BRCA pathway [16–19], but the impact of FA signaling on mitotic centrosome function per se has not been studied. At mitotic entry, maturing centrosomes nucleate microtubules to build the mitotic spindle [36]. These microtubules undergo controlled rearrangements to properly capture kinetochores before anaphase begins [37]. Because FANCA localizes to the mitotic apparatus [16,17], and FA signaling is implicated in the SAC [17], we wondered whether FANCA regulates the dynamic equilibrium of spindle microtubule assembly in early mitosis. We quantified the ability of primary patient-derived *FANCA−/−* and *FANCA+* fibroblasts to establish spindles in modified spindle assembly assays (Fig. 4A) [38]. Live cells were first placed at 4°C to destabilize microtubules (Fig. 4B) and then given prewarmed growth medium to stimulate spindle regrowth, fixed, and analyzed via quantitative deconvolution microscopy. Prometaphase *FANCA−/−* centrosomes demonstrated impaired spindle nucleating ability evidenced by the decreased

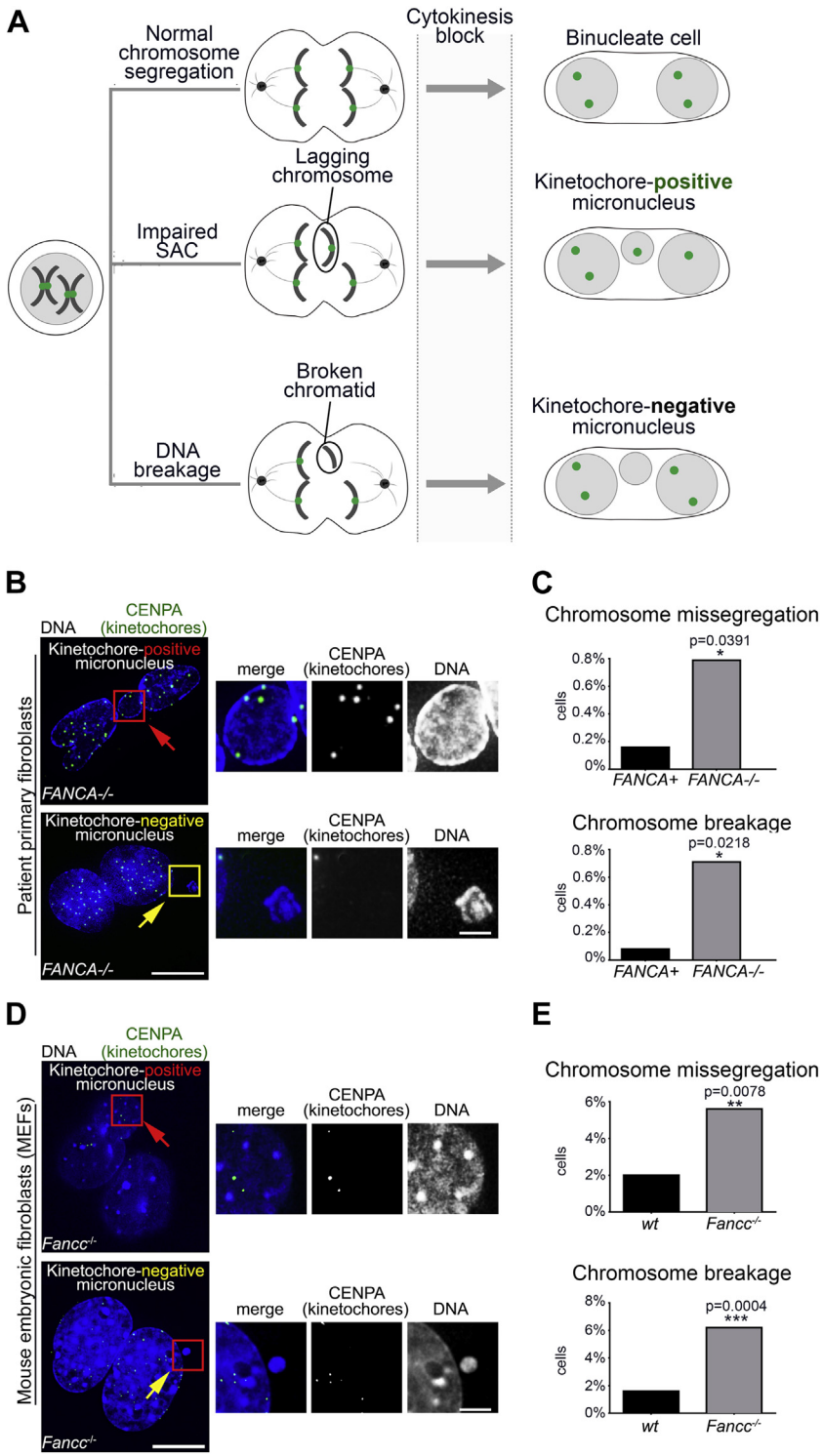

Figure 3. Micronucleation on loss of FA signaling results from a combination of interphase and mitotic errors. **(A)** Schematic of the cytokinesis-block micronucleus test, which discriminates the origin of aneuploidy based on the presence or absence of kinetochores within micronuclei. **(B)** Representative images of micronuclei in *FANCA–/–* primary patient fibroblasts. Bars = 10 μm (left) and 2 μm (right). **(C)** Quantification of micronuclei resulting from whole-chromosome missegregation versus chromosome breakage in primary *FANCA–/–* and *FANCA+* fibroblasts. Error bars represent means ± SEM. **(D)** Representative images of micronuclei in *Fancc–/–* MEFs. Scale bars = 10 μm (left) and 2 μm (right). **(E)** Quantification of micronucleation resulting from chromosome missegregation and chromosome breakage in wild-type and *Fancc –/–* MEFs. At least 260 cells were counted per condition; significance was determined with Student's *t* test. Cells were imaged with deconvolution microscopy (Applied Precision PersonalDx) and deconvolved with Softworx imaging suite (10 iterations, ratio: conservative).

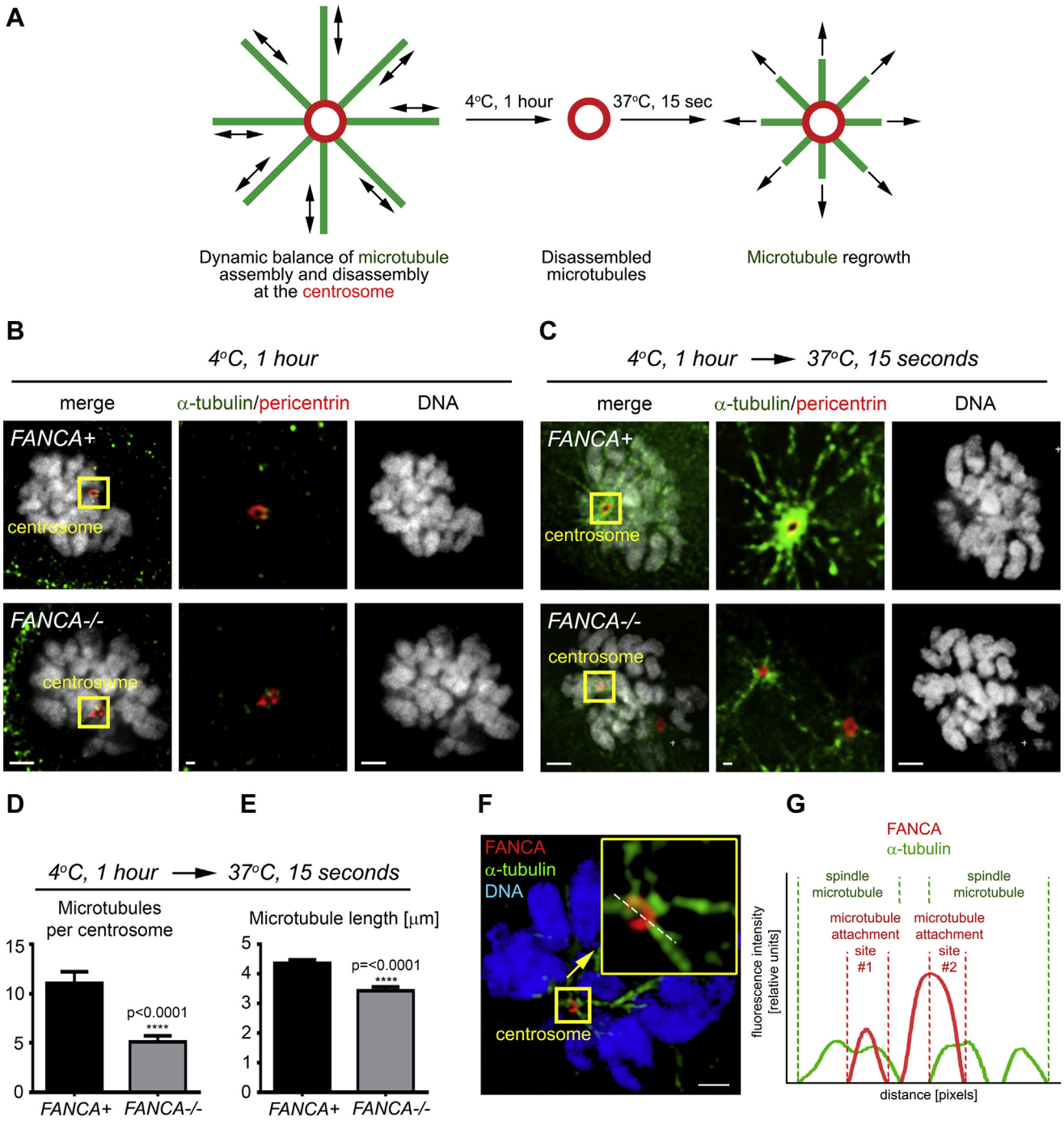

Figure 4. Loss of FANCA disrupts spindle microtubule assembly at prometaphase centrosomes. **(A)** Experiment design. Microtubules of living *FANCA–/–* and *FANCA+* cells were destabilized by cold treatment (4°C for 1 hour). Cells were then returned to 37°C to initiate microtubule reassembly and fixed with 4% paraformaldehyde 15 sec later. **(B)** Cold treatment fully destabilizes microtubules in *FANCA+* and *FANCA–/–* prometaphase cells. **(C)** Representative images of mitotic spindle assembly in *FANCA+* and *FANCA–/–* prometaphase cells stained with anti-α-tubulin (*green*) and anti-pericentrin (*red*) antibodies. Images were captured with 60× lens on the Deltavision deconvolution microscope. Scale bars = 2 μm (left and right) and 500 nm (region of interest in center). **(D, E)** Quantification of spindle microtubules per centrosome **(D)** and microtubule length (μm) **(E)** in gene-corrected and *FANCA–/–* cells treated as described in **(A)**. Data represent two independent experiments (n = 130 microtubules/experiment), and error bars represent SEM. **(F)** Representative mitotic HeLa cells stained with anti-FANCA (*red*) and anti-α-tubulin (*green*) antibodies, imaged on an ELYRA PS.1 super-resolution microscope using SIM technology. Inset: Enlarged centrosome-containing region of interest. *White dashed line* represents the line of fluorescence intensity profile. Bar = 2 μm. Cells were imaged with deconvolution microscopy (Applied Precision PersonalDx) and deconvolved with Softworx imaging suite (10 iterations, ratio: conservative). **(G)** Fluorescence intensity profiles of FANCA (*red*) and α-tubulin (*green*) signal.

number of microtubules emanating from each centrosome ($p \leq 0.0001$) (Fig. 4C, D). The spindle microtubules nucleated by *FANCA*−/− centrosomes were shorter ($p \leq 0.0001$) (Fig. 4E) than microtubules assembled in gene-corrected cells. Importantly, *FANCA*−/− cells containing supernumerary centrosomes [16,17] were excluded from the analysis. Therefore, FANCA is essential not only for the maintenance of centrosome number, but also for efficient mitotic spindle assembly. Super-resolution structured illumination microscopy (SR-SIM) revealed endogenous FANCA on mitotic centrosomes in close proximity to spindle microtubules (Fig. 4F, G), consistent with the role of FANCA in spindle dynamics.

FANCA shuttles to the pericentriolar material during mitotic centrosome maturation

Multiple FA proteins, including FANCA (Fig. 4F, G), localize to centrosomes and mitotic spindles [16–18]. However, it is unknown whether FANCA association with centrosomes changes between interphase and mitosis, as expected of a bona fide regulator of mitotic centrosome/spindle function [39,40].

Centrosome maturation prepares centrosomes for mitosis through reorganization of the pericentriolar material (PCM). A phosphosignaling circuit of cyclin-dependent kinases (CDKs), polo-like kinase 1 (PLK1), and Aurora A [41] recruits pericentrin [39] and γ-tubulin [40] to the PCM at mitotic entry to increase the spindle nucleating centrosome activity [42]. Because FANCA regulates spindle assembly (Fig. 4B–E), we wondered whether FANCA is recruited to the PCM of maturing centrosomes similar to these other centrosome-spindle regulators. To examine FANCA subcentrosomal localization, we employed deconvolution and super-resolution microscopy, which allows visualization of centrosomes beyond the diffraction limit imposed by conventional microscopes [43,44]. At mitotic entry, FANCA shuttled from centrioles toward the PCM and colocalized with pericentrin, γ-tubulin, and the minus end of spindle microtubules until the mitotic exit (Fig. 5A, B; Supplementary Figures E2–E5, online only, available at www.exphem.org). In interphase, FANCA returned to the mother centriole (Supplementary Figure E6, online only, available at www.exphem.org). These observations were confirmed with multiple primary antibodies and imaging of *FANCA*−/− patient cells stably expressing GFP-FANCA.

To thoroughly analyze FANCA distribution within the PCM, we analyzed individual 84-nm-thin super-resolution sections of mitotic centrosomes. At the mid-centrosome level, we observed well-organized FANCA fibers extending through and beyond the pericentrin-decorated PCM network from centrioles toward microtubule nucleation sites (Fig. 5B, C). This dynamic relocalization of FANCA to the PCM during mitosis supports the newly discovered role of FANCA in spindle microtubule nucleation (Fig. 4).

Loss of FANCA *allows escape from SAC arrest and apoptosis*

The FA/BRCA pathway repairs interphase DNA damage [45,46] and participates in the SAC [17]. To examine the fate of *FANCA*-deficient cells on SAC activation, we employed time-lapse imaging of primary *FANCA*−/− and gene-corrected cells treated with taxol, a microtubule-stabilizing chemotherapeutic agent (Fig. 6A). As described in other cells [47,48], *FANCA*-corrected, taxol-exposed cells entered prolonged prometaphase arrest followed by cell death without exiting mitosis. *FANCA*−/− cells were more likely to escape taxol-induced SAC arrest and generate multinucleated interphase-like cells ($p = 0.0215$) (Fig. 6B–E). These findings validate the role of FANCA in the SAC and indicate that loss of *FANCA* facilitates the escape of chromosomally unstable cells from mitotic death caused by unsatisfied SAC [47].

FANCA−/− *cells are hypersensitive to taxol*

A significant fraction of multinucleated cells that escape taxol-induced arrest [49] or form on failed mitosis [50,51] are physiologically eliminated to prevent genomic instability [26,52]. Complete SAC disruption causes chromosomal instability incompatible with cell survival [53]. Thus, we hypothesized that loss of *FANCA* may render cells hypersensitive to taxol.

As previous studies evaluating response of FA−/− cells to anti-mitotic chemotherapeutic agents generated conflicting data [16,54], we performed rigorous dose–response experiments to thoroughly examine this concept. We found that two separate *FANCA*−/− primary patient cell lines harboring different FANCA mutations are hypersensitive to taxol; stable FANCA expression rescued taxol hypersensitivity in both lines in two independent cell viability assays (Fig. 6F–H; Supplementary Figures E7 and E8, online only, available at www.exphem.org). Likewise, *FANCC*−/− primary fibroblasts displayed taxol hypersensitivity compared with *FANCC*-corrected cells (Supplementary Figure E8C). As expected [1,5], *FANCA*−/− and *FANCC*−/− cells exhibited decreased survival on exposure to the crosslinking agent MMC (Fig. 6F–H; Supplementary Figure E9, online only, available at www.exphem.org). These findings, together with previously published work [16], indicate that loss of FANCA or FANCC is synthetically lethal with exposure to anti-mitotic chemotherapeutic agents.

Chemotherapy-exposed FANCA−/− *cells develop distinct patterns of genomic instability because of separate interphase and mitotic checkpoint abnormalities*

Having established the hypersensitivity of FA−/− cells to interphase DNA crosslinkers and anti-mitotic agents, we wanted to understand how loss of FANCA confers hypersensitivity to these separate classes of chemotherapeutics.

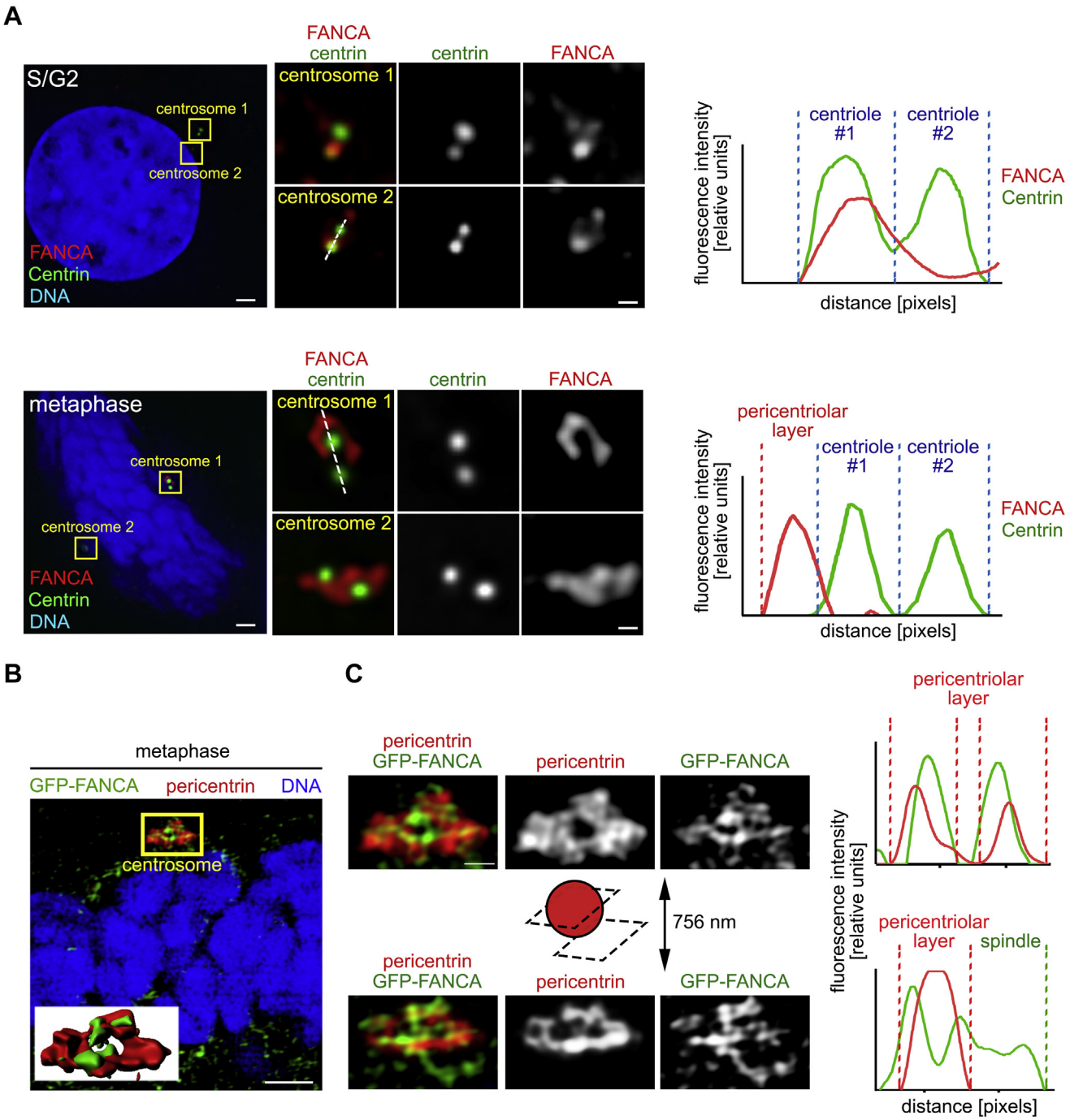

Figure 5. FANCA shuttles to the pericentriolar material during mitosis. **(A)** HeLa cells were immunostained with antibodies against endogenous FANCA (*red*) and centrin (*green*), imaged with deconvolution microscopy (Applied Precision PersonalDx) and deconvolved with Softworx imaging suite (10 iterations, ratio: conservative). Fluorescence intensity profiles indicate that FANCA co-localizes with centrin in interphase and migrates away from centrioles at metaphase. Bars = 1.5 μm (left) and 300 nm (right). **(B)** Representative super-resolution image of human fibroblast stably expressing GFP-FANCA and stained with antibody against the pericentriolar material marker (pericentrin). Inset: Three-dimensional rendering of the centrosome reveals co-localization of GFP-FANCA and pericentrin. Bar = 2 μm. The *yellow* region of interest is magnified **(C)** to show FANCA fibers embedded within the PCM (centrosome cross section) and extending toward the spindle (centrosome outer layer section). Fluorescence intensity profiles of GFP-FANCA/pericentrin signal at PCM and spindle are on the right. Bar = 500 nm. SR-SIM images were acquired on a Zeiss ELYRA PS.1 super-resolution microscopy system and exported using the Imaris imaging suite.

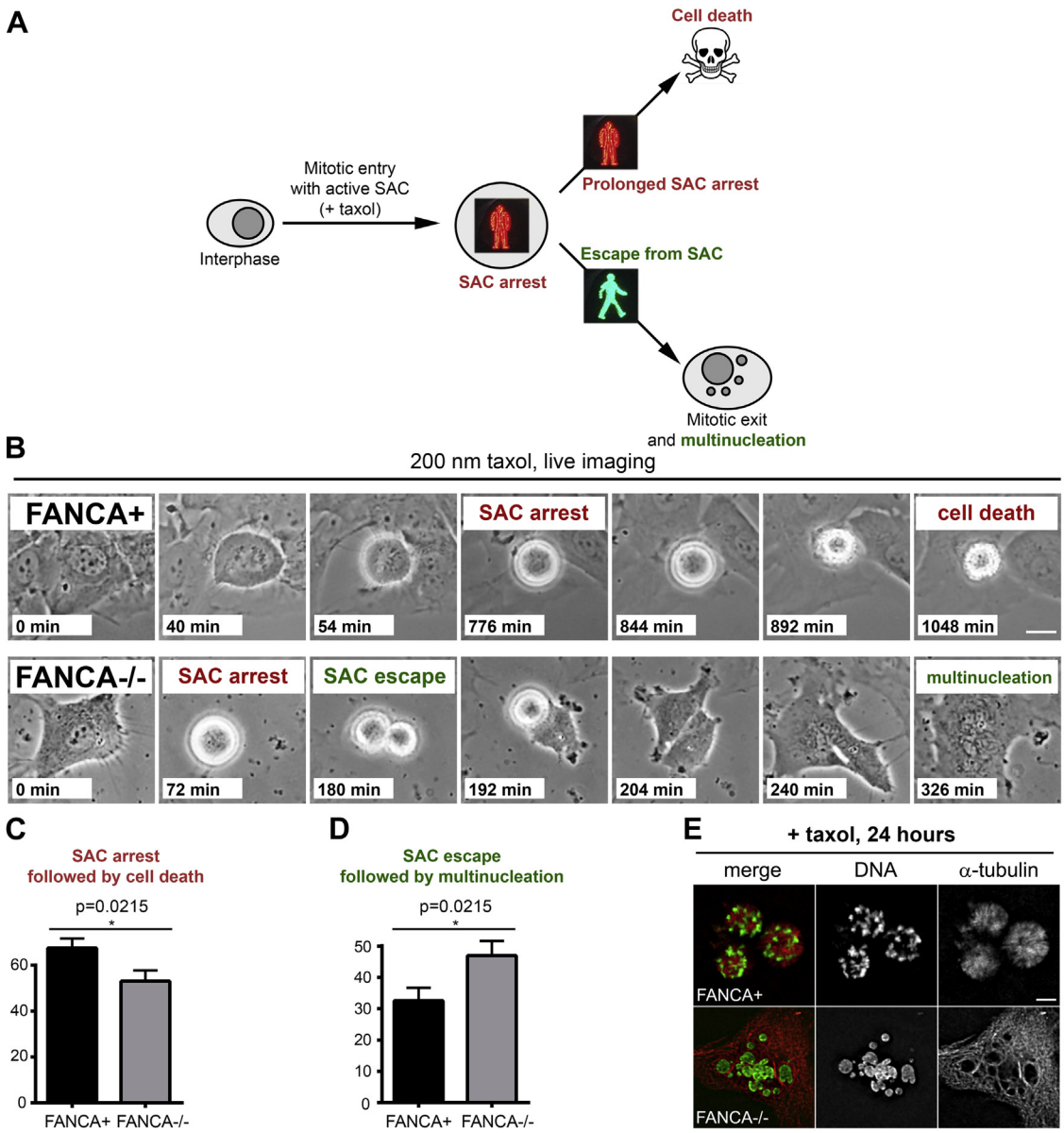

Figure 6. Loss of FANCA promotes escape from SAC and is synthetic lethal with low-dose taxol exposure. **(A)** Assay schematic. Prolonged activation of SAC triggers cell death to prevent genomic instability by eliminating cells that cannot satisfy the checkpoint. Escape from SAC followed by erratic chromosome segregation and mitotic exit generates multinucleated cells. **(B)** Representative time-lapse imaging snapshots of *FANCA*+ and *FANCA*–/– cells exposed to taxol. Note prolonged SAC arrest followed by cell death in gene-corrected cell and escape for SAC followed by cytokinesis failure and multinucleation in *FANCA*–/– cell. Bar = 15 μm. Time from mitotic entry is shown for each frame. Time-lapse phase-contrast frames of cells grown in DMSO supplemented with 10% FBS at 37°C, 5% CO_2 were acquired every 2 min for at least 24 hours on a Nikon Biostation live-imaging system **(C, D)** Quantification of time-lapse imaging experiments. *FANCA*–/– cells are more likely to escape SAC and less likely to be eliminated through SAC-associated death compared with gene-corrected isogenic cells ($p = 0.0215$). Data for 115 mitotic *FANCA*+ cells and 129 mitotic *FANCA*–/– cells (three experimental replicates for each cell line) were analyzed with a two-tailed *t* test (Supplementary Videos 1 and 2, online only, available at www.exphem.org). **(E)** Prolonged prometaphase arrest in FANCA+ cells and multinucleation in *FANCA*–/– cells on 24-hour exposure to taxol in an independent experiment. Images acquired on an Applied Precision PersonalDx deconvolution microscope.

Thus, we examined cell cycle and patterns of genomic instability in primary *FANCA*−/− and gene-corrected cells at baseline (Supplementary Figure E10, online only, available at www.exphem.org) and upon treatment with sublethal doses of MMC and taxol. We selected drug doses that decreased growth of *FANCA*−/− cells compared with isogenic *FANCA*+ cells without fully arresting *FANCA*−/− cells or inducing cell death evidenced by increased sub-G1 fraction on flow cytometry (Fig. 7A and not shown).

Prolonged treatment with 1 nmol/L MMC reduced growth of *FANCA*−/− cells as a result of persistent activation of the

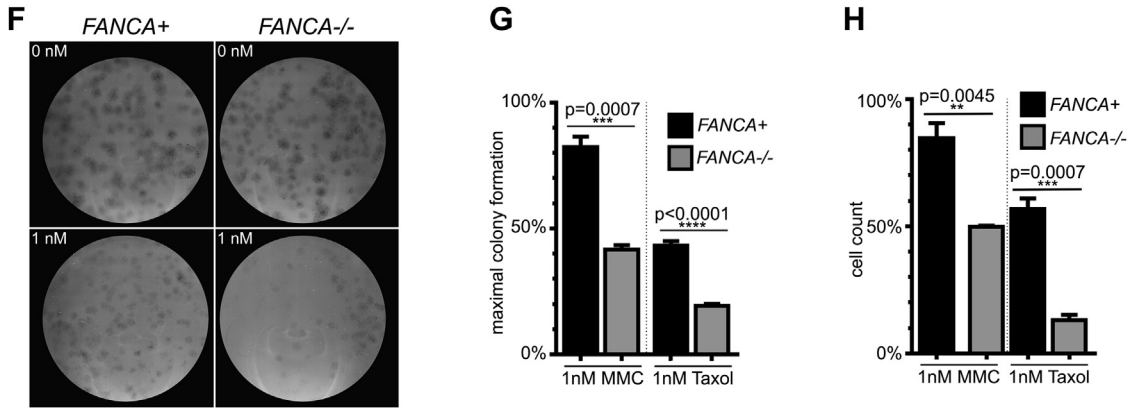

Figure 6. (*continued*) **(F)** Representative colony-forming unit (CFU) assay plates. Primary *FANCA–/–* fibroblasts and *FANCA+* fibroblasts (500 cells per 10-cm^2 plate) were exposed to taxol for 11 days. Note decreased colony formation on *FANCA–/–* plates exposed to 1 nmol/L taxol. **(G)** Quantification of the CFU assay in **(F)**. *FANCA–/–* cells are more sensitive to 1 nmol/L taxol than *FANCA+* cells in the CFU assay. MMC at 1 nmol/L was used as positive control. **(H)** Direct cell counts confirm that stable expression of FANCA rescues both taxol and MMC hypersensitivity of *FANCA–/–* patient cells. Two-way analysis of variance with Sidak correction was used for data comparison. Data represent pooled results of three separate experiments, expressed as means ± SEM in triplicates.

G2/M checkpoint ($p = 0.0376$), reflected by decreased DNA replication ($p < 0.0001$) and decreased G1 fraction ($p = 0.0029$) (Fig. 7A–D). This observation is consistent with the exaggerated MMC-induced G2/M arrest of FA cells caused by DDR failure [45,46]. In further support of this notion, exposure to low-dose MMC increased multinucleation resulting from DNA breakage ($p = 0.0223$), but not chromosome missegregation (Fig. 7E–G). Sublethal taxol exposure affected *FANCA−/−* cells differently. Prolonged treatment with low-dose taxol (but not MMC) significantly decreased the mitotic fraction of *FANCA−/−* cells compared with gene-corrected cells ($p < 0.0001$) (Fig. 7H, I), consistent with impaired SAC (Fig. 6). Furthermore, low-dose taxol increased multinucleation of *FANCA−/−* patient cells secondary to mitotic chromosome missegregation ($p < 0.0001$) as well as chromosome breakage ($p = 0.0059$) (Fig. 7J, K). Interestingly, multinucleated cells continued to enter S phase (Supplementary Figure E11, online only, available at www.exphem.org) [52,55].

In summary, these results (i) provide evidence that both impaired DDR and error-prone mitosis contribute to chromosomal instability in *FANCA−/−* cells in vivo and ex vivo, (ii) offer insights into the role of the FA pathway in the response to DNA-crosslinking agents and antimitotic chemotherapeutic agents, and (iii) open potential new inroads toward synthetic lethal chemotherapy against FA-deficient cancers.

Discussion

Disrupted FA/BRCA signaling causes genomic instability and cancer. The FA/BRCA tumor suppressor network orchestrates interphase DDR and DNA replication [1,5]. Multiple lines of evidence have implicated FA/BRCA signaling in centrosome maintenance and mitotic checkpoints [16–19,21,23], but the in vivo importance of these findings is unknown. We found that both abnormal interphase and error-prone mitosis significantly contribute to the in vivo hematopoietic genomic instability in FA−/− humans and mice, suggesting a role for the FA/BRCA network in genome surveillance throughout the cell cycle (Fig. 7L).

FANCA−/− patients' hematopoiesis is afflicted by mitotic errors. Lagging chromosomes caused by an in vivo SAC impairment [17] and persistent anaphase/telophase bridges [21,22] occur with increased frequency in *FANCA−/−* patients (Fig. 1). In agreement with the work from the D'Andrea group [23], binucleated hematopoietic cells (Fig. 1) are signs of faulty cytokinesis. Increased chromosome missegregation during erythropoiesis in *Fancc−/−* mice (Fig. 1D, E) indicates that other FA/BRCA proteins are essential for in vivo high-fidelity chromosome partition in hematopoietic cells in an evolutionarily conserved manner. The onset of FA-associated mitotic abnormalities precedes the MDS/AML (Fig. 1, Supplementary Table E1), suggesting that impaired mitosis may contribute to carcinogenesis in FA. Indeed, FISH analysis detected chromosomally unstable clones in 15% of FA patients with morphologically normal marrows [56], and gross chromosomal instability is a hallmark of MDS/AML in FA [57]. More research is needed to quantify the impact of haphazard mitosis on FA-associated myelodysplasia and cancer.

The irregular mitosis during FA−/− hematopoiesis is a consistent but relatively rare event (Figs. 1, 2). Further, although multinucleated cells with centrosome clusters are easily seen in FA-deficient cancer cells [17], multinucleation in FA−/− primary cells is more subtle (Figs. 2, 3) [17], perhaps because cancers cannot eliminate misdividing cells through backup checkpoints. Indeed, centrosome abnormalities induce TP53-dependent cell cycle arrest [51] and apoptosis [50], and activation of TP53 contributes to BMF in FA [58]. TP53 inactivation boosts hematopoiesis but

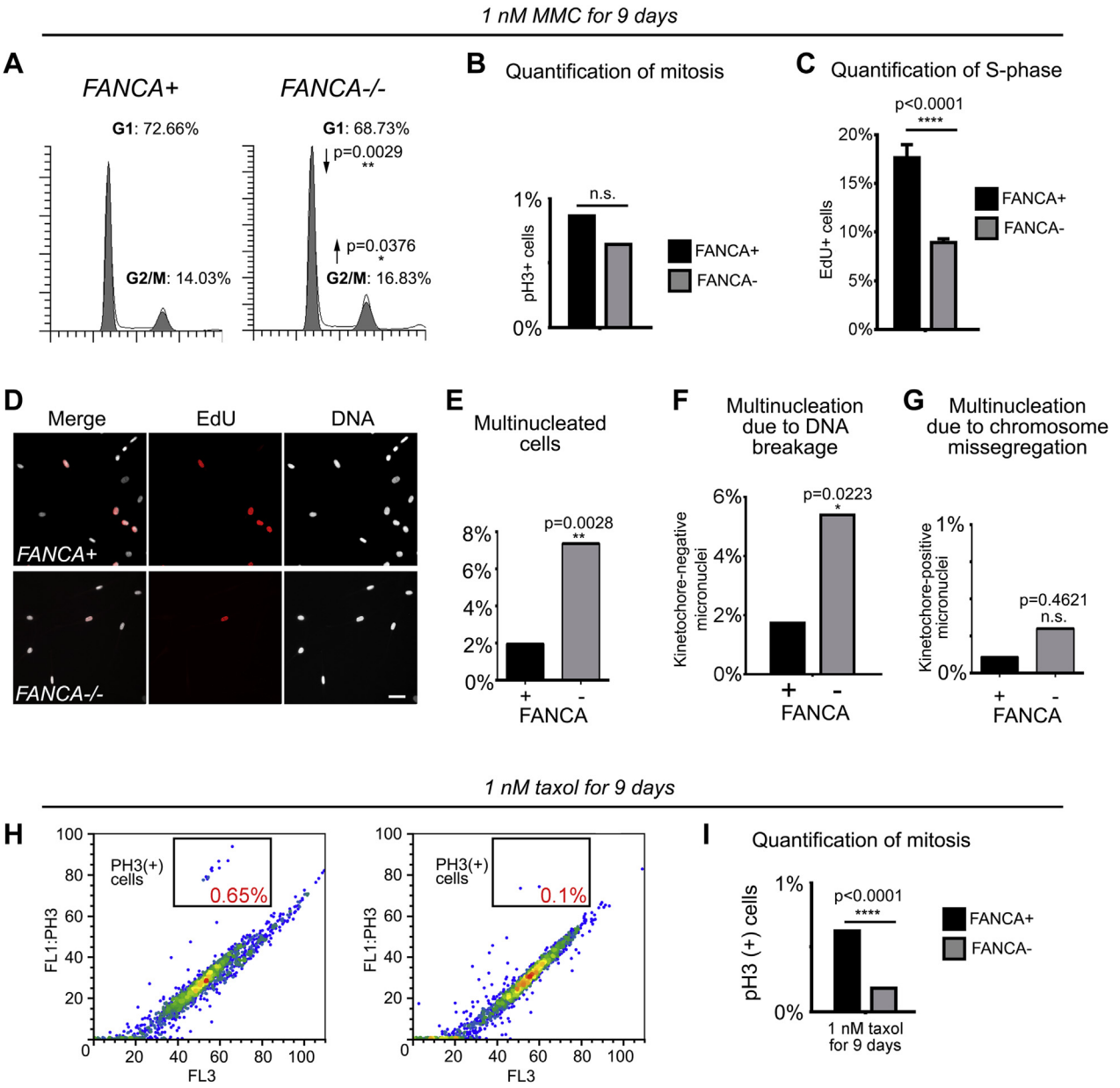

Figure 7. FANCA–/– cells exposed to genotoxic stressors develop genomic instability through a combination of interphase and mitotic checkpoint abnormalities. **(A)** Prolonged activation of the G2/M checkpoint in FANCA–/– cells grown in low-dose MMC for 9 days. **(B)** No difference in mitotic cell fraction between MMC-treated *FANCA–/–* and *FANCA+* cells indicates that the increased *FANCA–/–* G2/M fraction in **(A)** reflects G2 arrest prior to mitotic entry. **(C, D)** DNA replication arrest in *FANCA–/–* cells exposed to 1 nmol/L MMC is rescued by FANCA gene correction. S-Phase cells were labeled red by EdU incorporation. **(E–G)** Increased multinucleation caused by DNA breakage, but not chromosome missegregation, in *FANCA–/–* cells grown in low-dose MMC. **(H, I)** Flow cytometry reveals a decreased fraction of mitotic cells in *FANCA–/–* cells exposed to sublethal dose of taxol.

promotes MDS/AML in FA [59], and AML with bizarre karyotype instability occurred in an FA patient with somatic loss of heterozygosity of the TP53-harboring region of chromosome 17 [60]. Thus, aneuploidy and centrosome disruption on inactivation of FA/BRCA signaling may trigger TP53-dependent checkpoints to limit the risk of leukemia at the cost of BMF.

The role of FANCA in mitosis is not clearly defined. Impaired FA signaling promotes accumulation of centrosomes as a result of DDR-induced centrosome overreplication [18,19] and deregulated mitosis [17,23]. Supernumerary centrosomes promote chromosomal instability through multiple mechanisms [26,61]. We found that FANCA regulates centrosome-associated spindle assembly (Fig. 4), and FANCA shuttles from centrioles to the PCM spindle attachment sites at mitotic entry (Figs. 4 and 5). Dissecting FANCA-dependent mitotic centrosome–microtubule–kinetochore interactions in more detail will help

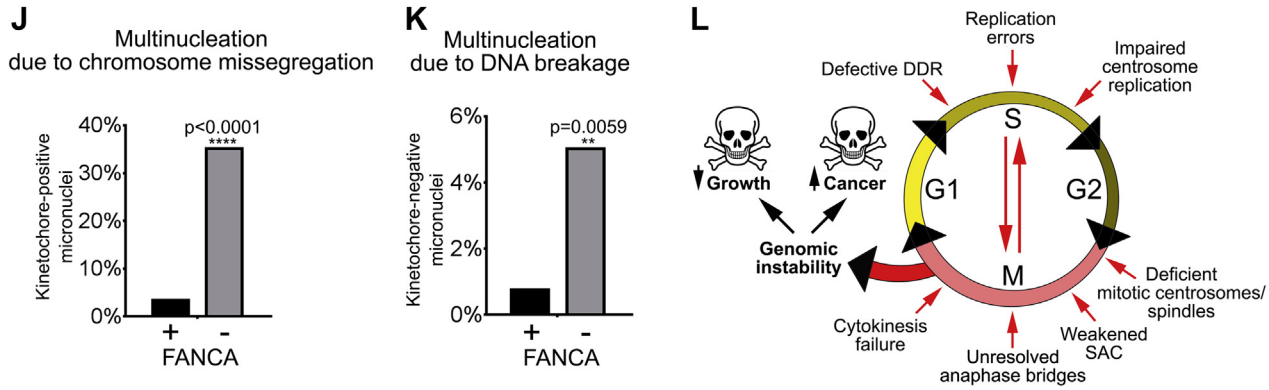

Figure 7. (*continued*) **(J, K)** Treatment with taxol increases chromosome segregation errors and chromosome breakage in *FANCA–/–* cells. **(L)** Compound interphase and mitotic origins of genomic instability in FA-deficient cells (see text for discussion). Exponential accumulation of DNA damage may result in activation of cell cycle arrest/apoptosis (bone marrow failure) or malignant transformation (leukemia and solid tumors). All flow cytometry data represent pooled three replicates for each cell line and condition compared with two-tailed *t* test. EdU incorporation counts were compared via two-way analysis of variance with Sidak's multiple comparison test.

understand how FANCA regulates the SAC [17]. We hypothesize that functional and numerical centrosome abnormalities in FA-deficient cells may further promote chromosomal instability by promoting merotelic kinetochore attachment to spindle microtubules; this mechanism of genomic instability has been elucidated in non-FA cells acquiring supernumerary centrosomes [61,62]. Interestingly, FANCA is phosphorylated by NIMA-related kinase 2 (NEK2) [16] and AKT kinase [63]; FANCJ and FANCD1 may regulate polo-like kinase 1 (PLK1) [18,19], which is essential for spindle function [64]; and FANCC binds the key mitotic cyclin-dependent kinase 1 (CDK1) [65], which coimmunoprecipitates with the FA core complex [66]. Moreover, loss of FANCA is synthetic lethal with PLK1 knockdown [67], and CDK inhibitors disrupt ionizing radiation-induced formation of FANCD2 foci [68]. Future work will examine these pathway connections to evaluate their translational relevance in cancer and FA.

We found that loss of FA signaling is synthetically lethal with taxol exposure, highlighting the role of FA-dependent SAC in cell survival. Kim et al. observed hypersensitivity of *FANCA*-knockdown cells to nocodazole [16]. Taxol and nocodazole are mechanistically different [69]: nocodazole disrupts spindle–kinetochore attachment, whereas taxol renders the attached microtubules unable to stretch the kinetochores. Because the FA pathway is essential for taxol- and nocodazole-induced SAC [17], FANCA may regulate SAC by intra-kinetochore tension.

Of note, others have found that *FANCG*/*FANCC*-deficient pancreatic cancer cells exposed to taxol accumulate DNA at a rate similar to that of gene-corrected cells in in vitro fluorescence assays [54], and concluded that FA−/− cells are not hypersensitive to anti-mitotic agents. However, FA−/− cells multinucleate (Fig. 6) [16,17] and replicate (Supplementary Figure E11, online only, available at www.exphem.org) on exposure to anti-mitotic agents, suggesting why cell growth assays quantify taxol response with better specificity than total DNA measurements. Interestingly, low-dose taxol promotes chromosome missegregation and DNA breaks in *FANCA*−/− cells. Consistent with this notion, the Pellman group demonstrated that micronuclei produced by mitotic errors undergo excessive mutagenesis [52] with secondary chromosome breakage [55] caused by erratic replication. The micronucleus-associated chromosome breakage may be further exacerbated by failed DDR in *FANCA*−/− micronuclei.

Micronucleation has been noted in FA for decades [70,71], but it was unclear whether it reflects interphase abnormalities or erratic mitoses. We addressed this question with quantitative high-resolution imaging-based micronucleation assays validated in previous studies [32]. Given the key role of FA signaling in interphase [1,5], we made an effort to confirm that kinetochore-containing micronuclei are not produced simply by impaired DDR. Importantly, the DNA-crosslinking agent (MMC) produced "DNA breakage" micronuclei, but not "chromosome missegregation" micronuclei (Fig. 7F, G), confirming the assay's specificity and sensitivity in distinguishing interphase from mitotic errors. Thus, we concluded that genomic instability results from DNA breakage *and* chromosome missegregation in multiple FA−/− hematopoietic and nonhematopoietic cell types (Figs. 2 and 3). On the basis of these and other findings [17], we propose that FANCA deficiency causes genomic instability through a dual mechanism of impaired interphase DDR/replication and defective mitosis [72] (Fig. 7L). This model explains the FA-associated patterns of genetic instability and hypersensitivity to both DNA-crosslinking and anti-mitotic agents. Interphase errors exacerbate mitotic abnormalities, and mitotic failure promotes interphase mutagenesis. Chromatid remnants generated through impaired DDR or replication are randomly segregated in mitosis. Defective midbody constriction [25] and cytokinesis [23] may shatter lagging chromosomes resulting from impaired SAC [17,73]

and break unresolved anaphase bridges [21,22]. After mitotic exit, cells may attempt to repair splintered DNA through chromothripsis, the mutagenic process of randomly reconnecting chromosome fragments via non-homologous end joining (NHEJ) [74–76]. Because FA−/− cells favor error-prone NHEJ over homologous recombination [77], chromothripsis may have a particularly detrimental impact on genomic stability on loss of the FA/BRCA network.

Our observations unveil the translational importance of mitotic defects caused by loss of FA/BRCA signaling. Somatic disruption of FA/BRCA genes occurs in malignancies in non-FA patients, including leukemia [12,13,78,79] and cervical [10], ovarian [11,80,81], breast [82], bladder [83], and lung [84] cancers. Our analysis of the COSMIC [85] database revealed multiple cancer-associated *FANCA* and *FANCC*-inactivating mutations in non-FA patients (Supplementary Figure E12, online only, available at www.exphem.org). As FA−/− cells are hypersensitive to anti-mitotic agents, future preclinical studies will determine whether targeting of mitosis can be employed in FA-deficient cancers. This strategy may complement other evidence-driven precision medicine efforts against FA−/− cancers, such as targeting of PARP-dependent DNA repair pathways [86–88], DNA damage kinases [89], and selective use of crosslinkers [11,68].

Acknowledgments

We are grateful to the Fanconi anemia patients and families who generously provided cells used in this study. Primary FA patient fibroblasts were a kind gift of Dr. Helmut Hanenberg and Dr. D. Wade Clapp (Indiana University). *Fancc−/−* mice were a generous gift of Dr. D. Wade Clapp (Indiana University). GN is supported by the NIH K12 Indiana Pediatric Scientist Award, by the Barth Syndrome/Bone Marrow Failure Research Fund at Riley Children's Foundation, and by the Heroes Foundation. DC was supported in part by Grant UL1TR001108 (A. Shekhar, PI) from the NIH, National Center for Advancing Translational Sciences, Clinical and Translational Science Award, and T32 HL007910 "Basic Science Studies on Gene Therapy of Blood Diseases" grant. ESP was supported by T32 Pediatric Clinical Pharmacology Fellowship (NIH: 5 T32 HD69047-2) and T32 HL007910 "Basic Science Studies on Gene Therapy of Blood Diseases" grants.

This work was presented in part at the American Society of Hematology 55th Annual Meeting in New Orleans, Louisiana, and at the American Society of Hematology 56th Annual Meeting in San Francisco, California.

Author contributions

ZAS and DC contributed equally to this work by performing experiments and editing the article. ESP, ZS, RE, and YH performed experiments. KR and WSG obtained patient specimens and institutional review board approval. G.N. designed the study, supervised data analysis, and wrote the article.

Conflict of interest disclosure

The authors declare that no conflicts of interest exist.

References

1. Kottemann MC, Smogorzewska A. Fanconi anaemia and the repair of Watson and Crick DNA crosslinks. Nature. 2013;493:356–363.
2. Rosenberg PS, Alter BP, Ebell W. Cancer risks in Fanconi anemia: Findings from the German Fanconi Anemia Registry. Haematologica. 2008;93:511–517.
3. Alter BP, Giri N, Savage SA, et al. Malignancies and survival patterns in the National Cancer Institute inherited bone marrow failure syndromes cohort study. Br J Haematol. 2010;150:179–188.
4. Alter BP. Fanconi anemia and the development of leukemia. Best Pract Res Clin Haematol. 2014;27:214–221.
5. D'Andrea AD. Susceptibility pathways in Fanconi's anemia and breast cancer. N Engl J Med. 2010;362:1909–1919.
6. Howlett NG, Taniguchi T, Olson S, et al. Biallelic inactivation of BRCA2 in Fanconi anemia. Science. 2002;297:606–609.
7. Sawyer SL, Tian L, Kahkonen M, et al. Biallelic mutations in BRCA1 cause a new Fanconi anemia subtype. Cancer Discov. 2015;5:135–142.
8. Jones S, Hruban RH, Kamiyama M, et al. Exomic sequencing identifies PALB2 as a pancreatic cancer susceptibility gene. Science. 2009;324:217.
9. Seal S, Thompson D, Renwick A, et al. Truncating mutations in the Fanconi anemia J gene BRIP1 are low-penetrance breast cancer susceptibility alleles. Nat Genet. 2006;38:1239–1241.
10. Narayan G, Arias-Pulido H, Nandula SV, et al. Promoter hypermethylation of FANCF: Disruption of Fanconi anemia–BRCA pathway in cervical cancer. Cancer Res. 2004;64:2994–2997.
11. Taniguchi T, Tischkowitz M, Ameziane N, et al. Disruption of the Fanconi anemia–BRCA pathway in cisplatin-sensitive ovarian tumors. Nat Med. 2003;9:5680574.
12. Tischkowitz M, Ameziane N, Waisfisz Q, et al. Bi-allelic silencing of the Fanconi anaemia gene FANCF in acute myeloid leukaemia. Br J Haematol. 2003;123:469–471.
13. Tischkowitz MD, Morgan NV, Grimwade D, et al. Deletion and reduced expression of the Fanconi anemia FANCA gene in sporadic acute myeloid leukemia. Leukemia. 2004;18:420–425.
14. Langevin F, Crossan GP, Rosado IV, Arends MJ, Patel KJ. Fancd2 counteracts the toxic effects of naturally produced aldehydes in mice. Nature. 2011;475:53–58.
15. Garaycoechea JI, Crossan GP, Langevin F, Daly M, Arends MJ, Patel KJ. Genotoxic consequences of endogenous aldehydes on mouse haematopoietic stem cell function. Nature. 2012;489:571–575.
16. Kim S, Hwang SK, Lee M, et al. Fanconi anemia complementation group A (FANCA) localizes to centrosomes and functions in the maintenance of centrosome integrity. Int J Biochem Cell Biol. 2013;45:1953–1961.
17. Nalepa G, Enzor R, Sun Z, et al. Fanconi anemia signaling network regulates the spindle assembly checkpoint. J Clin Invest. 2013;123:3839–3847.
18. Zou J, Tian F, Li J, et al. FancJ regulates interstrand crosslinker induced centrosome amplification through the activation of polo-like kinase 1. Biol Open. 2013;2:1022–1031.
19. Zou J, Zhang D, Qin G, Chen X, Wang H, Zhang D. BRCA1 and FancJ cooperatively promote interstrand crosslinker induced centrosome amplification through the activation of polo-like kinase 1. Cell Cycle. 2014;13:3685–3697.
20. London N, Biggins S. Signalling dynamics in the spindle checkpoint response. Nat Rev Mol Cell Biol. 2014;15:736–747.
21. Naim V, Rosselli F. The FANC pathway and BLM collaborate during mitosis to prevent micro-nucleation and chromosome abnormalities. Nat Cell Biol. 2009;11:761–768.
22. Chan KL, Palmai-Pallag T, Ying S, Hickson ID. Replication stress induces sister-chromatid bridging at fragile site loci in mitosis. Nat Cell Biol. 2009;11:753–760.
23. Vinciguerra P, Godinho SA, Parmar K, Pellman D, D'Andrea AD. Cytokinesis failure occurs in Fanconi anemia pathway-deficient

murine and human bone marrow hematopoietic cells. J Clin Invest. 2010;120:3834–3842.
24. Daniels MJ, Wang Y, Lee M, Venkitaraman AR. Abnormal cytokinesis in cells deficient in the breast cancer susceptibility protein BRCA2. Science. 2004;306:876–879.
25. Mondal G, Rowley M, Guidugli L, Wu J, Pankratz VS, Couch FJ. BRCA2 localization to the midbody by filamin A regulates cep55 signaling and completion of cytokinesis. Dev Cell. 2012;23:137–152.
26. Gordon DJ, Resio B, Pellman D. Causes and consequences of aneuploidy in cancer. Nat Rev Genet. 2012;13:189–203.
27. Hanahan D, Weinberg RA. Hallmarks of cancer: The next generation. Cell. 2011;144:646–674.
28. Bakhoum SF, Compton DA. Chromosomal instability and cancer: A complex relationship with therapeutic potential. J Clin Invest. 2012;122:1138–1143.
29. Chen M, Tomkins DJ, Auerbach W, et al. Inactivation of Fac in mice produces inducible chromosomal instability and reduced fertility reminiscent of Fanconi anaemia. Nat Genet. 1996;12:448–451.
30. Cammerer Z, Schumacher MM, Kirsch-Volders M, Suter W, Elhajouji A. Flow cytometry peripheral blood micronucleus test in vivo: Determination of potential thresholds for aneuploidy induced by spindle poisons. Environ Mol Mutagen. 2010;51:278–284.
31. Balmus G, Karp NA, Ng BL, Jackson SP, Adams DJ, McIntyre RE. A high-throughput in vivo micronucleus assay for genome instability screening in mice. Nat Protoc. 2015;10:205–215.
32. Fenech M. Cytokinesis-block micronucleus cytome assay. Nat Protoc. 2007;2:1084–1104.
33. Palmer DK, O'Day K, Trong HL, Charbonneau H, Margolis RL. Purification of the centromere-specific protein CENP-A and demonstration that it is a distinctive histone. Proc Natl Acad Sci USA. 1991;88:3734–3738.
34. Sigoillot FD, Lyman S, Huckins JF, et al. A bioinformatics method identifies prominent off-targeted transcripts in RNAi screens. Nat Methods. 2012;9:363–366.
35. Schuler M, Rupa DS, Eastmond DA. A critical evaluation of centromeric labeling to distinguish micronuclei induced by chromosomal loss and breakage in vitro. Mutat Res. 1997;392:81–95.
36. Brownlee CW, Rogers GC. Show me your license, please: Deregulation of centriole duplication mechanisms that promote amplification. Cell Mol Life Sci. 2013;70:1021–1034.
37. Godek KM, Kabeche L, Compton DA. Regulation of kinetochore–microtubule attachments through homeostatic control during mitosis. Nat Rev Mol Cell Biol. 2015;16:57–64.
38. O'Rourke BP, Gomez-Ferreria MA, Berk RH, et al. Cep192 controls the balance of centrosome and non-centrosomal microtubules during interphase. PLoS One. 2014;9:e101001.
39. Lee K, Rhee K. PLK1 phosphorylation of pericentrin initiates centrosome maturation at the onset of mitosis. J Cell Biol. 2011;195:1093–1101.
40. Sdelci S, Schutz M, Pinyol R, et al. Nek9 phosphorylation of NEDD1/GCP-WD contributes to Plk1 control of gamma-tubulin recruitment to the mitotic centrosome. Curr Biol. 2012;22:1516–1523.
41. Joukov V, Walter JC, De Nicolo A. The Cep192-organized aurora A-Plk1 cascade is essential for centrosome cycle and bipolar spindle assembly. Mol Cell. 2014;55:578–591.
42. Zimmerman WC, Sillibourne J, Rosa J, Doxsey SJ. Mitosis-specific anchoring of gamma tubulin complexes by pericentrin controls spindle organization and mitotic entry. Mol Biol Cell. 2004;15:3642–3657.
43. Lawo S, Hasegan M, Gupta GD, Pelletier L. Subdiffraction imaging of centrosomes reveals higher-order organizational features of pericentriolar material. Nat Cell Biol. 2012;14:1148–1158.
44. Mennella V, Agard DA, Huang B, Pelletier L. Amorphous no more: Subdiffraction view of the pericentriolar material architecture. Trends Cell Biol. 2014;24:188–197.
45. Chandra S, Levran O, Jurickova I, et al. A rapid method for retrovirus-mediated identification of complementation groups in Fanconi anemia patients. Mol Ther. 2005;12:976–984.
46. Heinrich MC, Hoatlin ME, Zigler AJ, et al. DNA cross-linker-induced G2/M arrest in group C Fanconi anemia lymphoblasts reflects normal checkpoint function. Blood. 1998;91:275–287.
47. Woods CM, Zhu J, McQueney PA, Bollag D, Lazarides E. Taxol-induced mitotic block triggers rapid onset of a p53-independent apoptotic pathway. Mol Med. 1995;1:506–526.
48. Jordan MA, Wendell K, Gardiner S, Derry WB, Copp H, Wilson L. Mitotic block induced in HeLa cells by low concentrations of paclitaxel (Taxol) results in abnormal mitotic exit and apoptotic cell death. Cancer Res. 1996;56:816–825.
49. Torres K, Horwitz SB. Mechanisms of Taxol-induced cell death are concentration dependent. Cancer Res. 1998;58:3620–3626.
50. Cuomo ME, Knebel A, Morrice N, Paterson H, Cohen P, Mittnacht S. p53-Driven apoptosis limits centrosome amplification and genomic instability downstream of NPM1 phosphorylation. Nat Cell Biol. 2008;10:723–730.
51. Mikule K, Delaval B, Kaldis P, Jurcyzk A, Hergert P, Doxsey S. Loss of centrosome integrity induces p38–p53–p21-dependent G1-S arrest. Nat Cell Biol. 2007;9:160–170.
52. Crasta K, Ganem NJ, Dagher R, et al. DNA breaks and chromosome pulverization from errors in mitosis. Nature. 2012;482:53–58.
53. Dobles M, Liberal V, Scott ML, Benezra R, Sorger PK. Chromosome missegregation and apoptosis in mice lacking the mitotic checkpoint protein Mad2. Cell. 2000;101:635–645.
54. Van der Heijden MS, Brody JR, Dezentje DA, et al. In vivo therapeutic responses contingent on Fanconi anemia/BRCA2 status of the tumor. Clin Cancer Res. 2005;11:7508–7515.
55. Zhang CZ, Spektor A, Cornils H, et al. Chromothripsis from DNA damage in micronuclei. Nature. 2015;522:179–184.
56. Mehta PA, Harris RE, Davies SM, et al. Numerical chromosomal changes and risk of development of myelodysplastic syndrome—Acute myeloid leukemia in patients with Fanconi anemia. Cancer Genet Cytogenet. 2010;203:180–186.
57. Quentin S, Cuccuini W, Ceccaldi R, et al. Myelodysplasia and leukemia of Fanconi anemia are associated with a specific pattern of genomic abnormalities that includes cryptic RUNX1/AML1 lesions. Blood. 2011;117:e161–e170.
58. Ceccaldi R, Parmar K, Mouly E, et al. Bone marrow failure in Fanconi anemia is triggered by an exacerbated p53/p21 DNA damage response that impairs hematopoietic stem and progenitor cells. Cell Stem Cell. 2012;11:36–49.
59. Ceccaldi R, Briot D, Larghero J, et al. Spontaneous abrogation of the G(2)DNA damage checkpoint has clinical benefits but promotes leukemogenesis in Fanconi anemia patients. J Clin Invest. 2011;121:184–194.
60. Woo HI, Kim HJ, Lee SH, Yoo KH, Koo HH, Kim SH. Acute myeloid leukemia with complex hypodiploidy and loss of heterozygosity of 17p in a boy with Fanconi anemia. Ann Clin Lab Sci. 2011;41:66–70.
61. Ganem NJ, Godinho SA, Pellman D. A mechanism linking extra centrosomes to chromosomal instability. Nature. 2009;460:278–282.
62. Nam HJ, Naylor RM, van Deursen JM. Centrosome dynamics as a source of chromosomal instability. Trends Cell Biol. 2015;25:65–73.
63. Otsuki T, Nagashima T, Komatsu N, et al. Phosphorylation of Fanconi anemia protein, FANCA, is regulated by Akt kinase. Biochem Biophys Res Commun. 2002;291:628–634.
64. Sumara I, Gimenez-Abian JF, Gerlich D, et al. Roles of polo-like kinase 1 in the assembly of functional mitotic spindles. Curr Biol. 2004;14:1712–1722.
65. Kupfer GM, Yamashita T, Naf D, Suliman A, Asano S, D'Andrea AD. The Fanconi anemia polypeptide, FAC, binds to the cyclin-dependent kinase, cdc2. Blood. 1997;90:1047–1054.

66. Thomashevski A, High AA, Drozd M, et al. The Fanconi anemia core complex forms four complexes of different sizes in different subcellular compartments. J Biol Chem. 2004;279:26201–26209.
67. Kennedy RD, Chen CC, Stuckert P, et al. Fanconi anemia pathway-deficient tumor cells are hypersensitive to inhibition of ataxia telangiectasia mutated. J Clin Invest. 2007;117:1440–1449.
68. Jacquemont C, Simon JA, D'Andrea AD, Taniguchi T. Non-specific chemical inhibition of the Fanconi anemia pathway sensitizes cancer cells to cisplatin. Mol Cancer. 2012;11:26.
69. Maresca TJ, Salmon ED. Welcome to a new kind of tension: Translating kinetochore mechanics into a wait-anaphase signal. J Cell Sci. 2010;123(Pt 6):825–835.
70. Barton JC, Parmley RT, Carroll AJ, et al. Preleukemia in Fanconi's anemia: Hematopoietic cell multinuclearity, membrane duplication, and dysgranulogenesis. J Submicrosc Cytol. 1987;19:355–364.
71. Willingale-Theune J, Schweiger M, Hirsch-Kauffmann M, Meek AE, Paulin-Levasseur M, Traub P. Ultrastructure of Fanconi anemia fibroblasts. J Cell Sci. 1989;93(Pt 4):651–665.
72. Nalepa G, Clapp DW. Fanconi anemia and the cell cycle: New perspectives on aneuploidy. F1000Prime Rep. 2014;6:23.
73. Choi E, Park PG, Lee HO, et al. BRCA2 fine-tunes the spindle assembly checkpoint through reinforcement of BubR1 acetylation. Dev Cell. 2012;22:295–308.
74. Maher CA, Wilson RK. Chromothripsis and human disease: Piecing together the shattering process. Cell. 2012;148:29–32.
75. Zhang CZ, Leibowitz ML, Pellman D. Chromothripsis and beyond: Rapid genome evolution from complex chromosomal rearrangements. Genes Dev. 2013;27:2513–2530.
76. Forment JV, Kaidi A, Jackson SP. Chromothripsis and cancer: Causes and consequences of chromosome shattering. Nat Rev Cancer. 2012;12:663–670.
77. Adamo A, Collis SJ, Adelman CA, et al. Preventing nonhomologous end joining suppresses DNA repair defects of Fanconi anemia. Mol Cell. 2010;39:25–35.
78. Hess CJ, Ameziane N, Schuurhuis GJ, et al. Hypermethylation of the FANCC and FANCL promoter regions in sporadic acute leukaemia. Cell Oncol. 2008;30:299–306.
79. Xie Y, de Winter JP, Waisfisz Q, et al. Aberrant Fanconi anaemia protein profiles in acute myeloid leukaemia cells. Br J Haematol. 2000;111:1057–1064.
80. Wang Z, Li M, Lu S, Zhang Y, Wang H. Promoter hypermethylation of FANCF plays an important role in the occurrence of ovarian cancer through disrupting Fanconi anemia–BRCA pathway. Cancer Biol Ther. 2006;5:256–260.
81. Olopade OI, Wei M. FANCF methylation contributes to chemoselectivity in ovarian cancer. Cancer Cell. 2003;3:417–420.
82. Wei M, Xu J, Dignam J, et al. Estrogen receptor alpha, BRCA1, and FANCF promoter methylation occur in distinct subsets of sporadic breast cancers. Breast Cancer Res Treat. 2008;111:113–120.
83. Neveling K, Kalb R, Florl AR, et al. Disruption of the FA/BRCA pathway in bladder cancer. Cytogenet Genome Res. 2007;118:166–176.
84. Marsit CJ, Liu M, Nelson HH, Posner M, Suzuki M, Kelsey KT. Inactivation of the Fanconi anemia/BRCA pathway in lung and oral cancers: Implications for treatment and survival. Oncogene. 2004;23:1000–1004.
85. Forbes SA, Beare D, Gunasekaran P, et al. COSMIC: exploring the world's knowledge of somatic mutations in human cancer. Nucleic Acids Res. 2015;43(Database issue):D805–D811.
86. Ceccaldi R, Liu JC, Amunugama R, et al. Homologous-recombination-deficient tumours are dependent on Poltheta-mediated repair. Nature. 2015;518:258–262.
87. Bryant HE, Schultz N, Thomas HD, et al. Specific killing of BRCA2-deficient tumours with inhibitors of poly(ADP-ribose) polymerase. Nature. 2005;434:913–917.
88. Farmer H, McCabe N, Lord CJ, et al. Targeting the DNA repair defect in BRCA mutant cells as a therapeutic strategy. Nature. 2005;434:917–921.
89. Chen CC, Kennedy RD, Sidi S, Look AT, D'Andrea A. CHK1 inhibition as a strategy for targeting Fanconi anemia (FA) DNA repair pathway deficient tumors. Mol Cancer. 2009;8:24.

Supplementary methods

Immunoblotting

For detection of FANCA protein expression, CD34+ cells were lysed in M-Per buffer (Thermo Scientific) containing phosphatase and protease inhibitors (Roche), and protein concentration was determined by BCA (Pierce). Fifteen micrograms of protein was loaded per well in a 4%–12% gradient Bis-Tris gel (Life Tech). Blots were blocked in 5% milk for 1 hour, then incubated overnight with anti-FANCA antibody (ab5063, Abcam) diluted 1:2,000 in 5% milk. Blots were washed with 0.1% Tween 20 in PBS (PBS-T) and incubated with anti-rabbit IgG horseradish peroxidase-linked secondary antibody diluted in PBS-T and 0.5% milk. Signal was detected via the enhanced chemiluminescence system (Life Tech).

CD34+ CFU assay

Transduced CD34+ cells were grown in triplicate (2,500 cells/35 mm dish) in Methocult (H4434) methylcellulose-based medium containing recombinant cytokines (Stem Cell) and varying concentrations of MMC. Plates were incubated at 37°C, 5% O_2 for 11 days. Colonies were then counted and defined as clusters of >50 cells.

Flow cytometry

To detect functional correction of isogenic-corrected patient fibroblasts, cells were treated for 48 hours with 33 nmol/L MMC and then harvested on incubation with HyClone HyQTase (Fisher) detachment solution for 15 min. Cells were pelleted and resuspended dropwise in cold 70% ethanol and stored at –20°C overnight. The following day, cells were spun down and resuspended in FxCycle PI/RNase Staining Solution (Life Tech) for cell cycle analysis.

For quantification of mitotic cells, fibroblasts were treated with 1 nmol/L MMC or 1 nmol/L taxol for 9 days. Cells were then removed from tissue culture plates on incubation with HyClone HyQTase (Fisher) detachment solution for 15 min at 37°C followed by 4% paraformaldehyde/PBS fixation for 10 min. Cells were pelleted, resuspended in 90% methanol, and stored at –20°C overnight. The next day, cells were incubated in 0.5% BSA/PBS for 4 min, pelleted, and stained with an Alexa Fluor 488-conjugated phospho-histone H3 antibody (Cell Signaling) diluted 1:50 in 0.5% BSA/PBS for 1 hour in the dark. The cells were next washed with PBS and analyzed on a FacsCalibur flow cytometer (Becton-Dickinson). Flow cytometry data analysis was performed using Flow Jo software.

S-Phase quantification

Cells grown on coverslips were treated for 9 days with 1 nmol/L MMC or 1 nmol/L taxol as described above, pulsed with EdU using the Click-iT EdU Imaging Kit (Life Technologies) for 45 min, then fixed and stained according to the manufacturer's protocol. Nuclei were counterstained with Hoechst 33342. Cells were imaged on the Deltavision deconvolution microscope, and the fraction of EdU-positive nuclei was manually quantified.

Generation of MEFs

To generate MEFs, *Fancc*+/– animals were intercrossed, and pregnant female mice from timed matings were sacrificed at day E13.5-14.5. Individual embryos were removed from the uterus, and then the tail and liver region of each embryo were removed. The head was also removed for polymerase chain reaction genotyping. Remaining embryo tissue was minced using a sterile razor blade and incubated with 1 mL 0.25% trypsin–EDTA (Life Technologies) for 10 min at 37°C in a 10-cm tissue culture dish. Next, 2 mL of growth medium was added, and the tissue was disaggregated into a single-cell suspension by repeated passage through a 16-gauge needle attached to a 3-mL syringe (Becton Dickinson). Eight milliliters of growth medium was then added to the plate, and MEFs were further cultured as described above. For all experiments, passage 2 MEFs were used.

Clonogenic (CFU) assays and direct cell count assays

Cells of the indicated genotypes were plated on 10-cm cell culture dishes (500 cells/plate). MMC or taxol (purchased from Sigma) was added to the growth medium 24 hours later. Plates were cultured in a 5% oxygen incubator for 11 days, then fixed and stained with 0.4% methylene blue–methanol to manually count colonies. A colony was defined as ≥ 50 cells/group. Plates were scanned using an Epson color scanner. For direct cell counting, six-well plates were seeded with 1×10^5 cells/well and treated with the indicated doses of MMC or taxol for 9 days. Cell counts were performed using a hemocytometer.

Bioinformatics analysis of cancer-associated FA mutations

Somatic cancer-associated mutations of *FANCA* and *FANCC* were identified within the COSMIC database [1]. The functional impact of mutations was examined with Mutation Assessor algorithm; mutations producing a functional impact score (FIS) >1.938 were considered potentially disruptive [2].

Live imaging

Cells were plated at 20,000 cells per quadrant in a 35-mm Hi-Q4 (Ibidi) culture dish. After 2 days, taxol was added (final concentration = 200 nm), and time-lapse phase-contrast images (5 z sections, total = 10 μm) were acquired every 2 min for a period of 48 hours using a BioStation IM-Q time-lapse imaging system (Nikon) equipped with a 20× 0.8 NA Plan Fluor objective lens. NIS-Elements AR Analysis 4.10.02 or NIS-Elements Viewer 4.20 microscope imaging software (Nikon) was used for video analysis. Videos were exported via Imaris (Bitplane) and Adobe Photoshop.

Antibodies used for immunofluorescence

The following primary antibodies were used in this study: rabbit anti-CENPA (Cell Signaling, 1:200), mouse anti-α-tubulin (Cell Signaling, 1:100), rabbit antipericentrin (Abcam, 1:100), mouse anticentrin 3 (Santa Cruz, 1:100), mouse anti-γ-tubulin (Abcam, 1:100), rabbit anti-CEP170 (Abcam, 1:100), as well as rabbit anti-FANCA (Abcam). Alexa 488- and Alexa 594-conjugated antibodies (Life Technologies) were used for primary antibody detection.

Supplementary Video E1. Primary FANCA−/− patient cell escapes taxol-induced spindle checkpoint arrest and exits mitosis to generate one giant multinucleated cell after failed cytokinesis.

Supplementary Video E2. FANCA gene correction rescues the spindle assembly checkpoint in FA patient-derived cell. Note prolonged taxol-induced mitotic arrest followed by cell death.

Supplementary Table E1. *Fancc*−/− mice have normal peripheral blood counts at 12 weeks of age[a]

	Peripheral blood count		
	Wild type	*Fancc*−/−	*p* Value
White blood cells (K/μL)	16.26 ± 1.285	18.19 ± 1.069	0.2548
Hemoglobin (g/dL)	14.49 ± 0.508	15.08 ± 0.1863	0.2574
Platelets (K/μL)	1,053 ± 70.96	1,111 ± 62.97	0.5440

[a]No erythroblasts or myeloblasts were noted on manual review of any *Fancc*−/− or wild-type mice at 3 months of age (n > 10 mice per genotype). Values are means ± SEM of 15 animals/group. *p* Values were obtained with an unpaired Student *t* test.

Supplementary References

1. Forbes SA, Beare D, Gunasekaran P, et al. COSMIC: Exploring the world's knowledge of somatic mutations in human cancer. Nucleic Acids Res. 2015;43(Database issue):D805–D811.
2. Reva B, Antipin Y, Sander C. Predicting the functional impact of protein mutations: Application to cancer genomics. Nucleic Acids Res. 2011;39:e118.
3. Heinrich MC, Hoatlin ME, Zigler AJ, et al. DNA cross-linker-induced G2/M arrest in group C Fanconi anemia lymphoblasts reflects normal checkpoint function. Blood. 1998;91:275–287.
4. Chandra S, Levran O, Jurickova I, et al. A rapid method for retrovirus-mediated identification of complementation groups in Fanconi anemia patients. Mol Ther. 2005;12:976–984.
5. Nalepa G, Enzor R, Sun Z, et al. Fanconi anemia signaling network regulates the spindle assembly checkpoint. J Clin Invest. 2013;123:3839–3847.
6. Crasta K, Ganem NJ, Dagher R, et al. DNA breaks and chromosome pulverization from errors in mitosis. Nature. 2012;482:53–58.
7. Zhang CZ, Spektor A, Cornils H, et al. Chromothripsis from DNA damage in micronuclei. Nature. 2015;522:179–184.

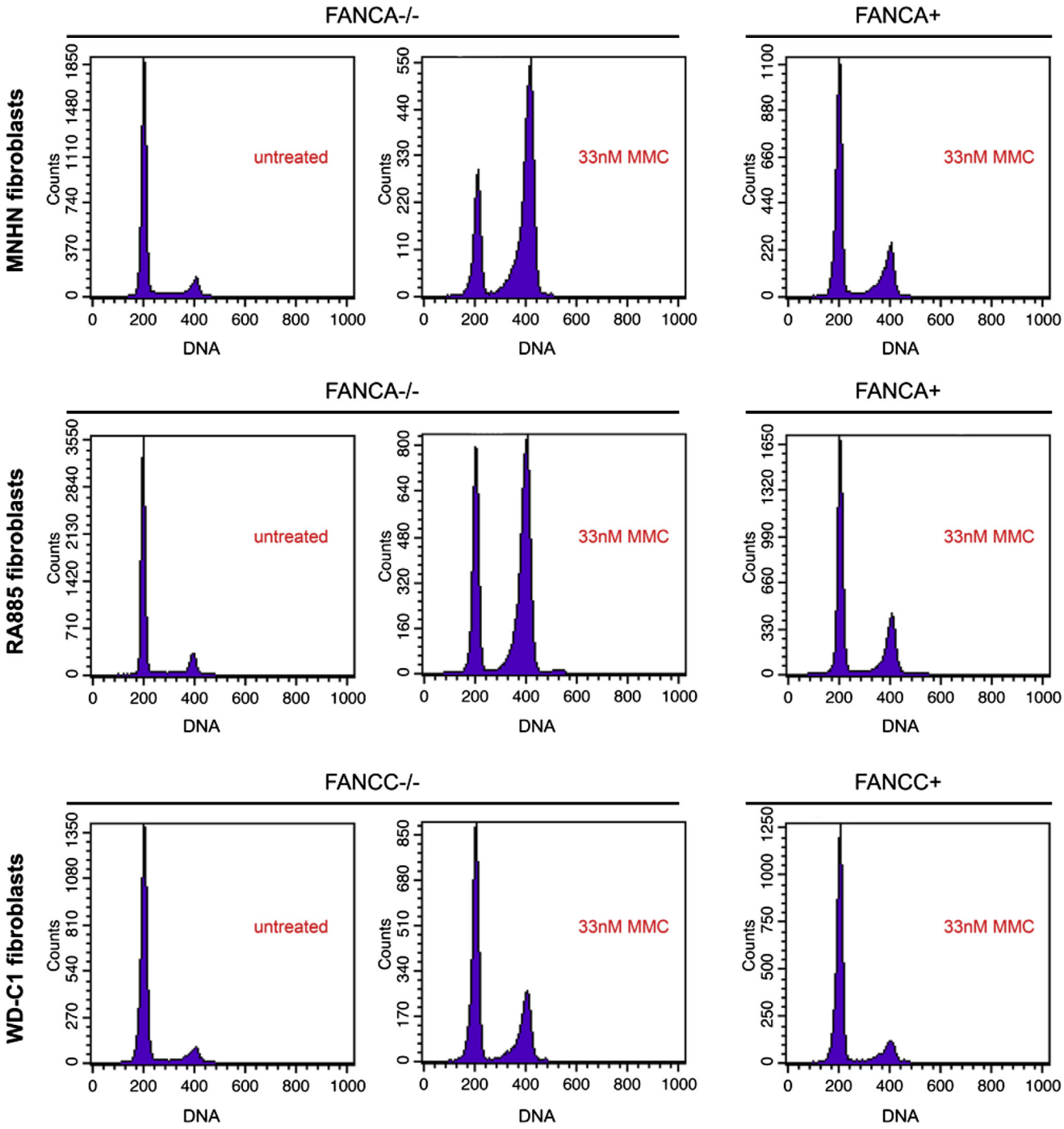

Supplementary Figure E1. Functional validation of FANCA and FANCC isogenic gene correction of primary patient fibroblasts. Cell cycle flow profiles of FANCA-deficient patient line MNHN (top), FANCA-deficient patient line RA885 (middle), and FANCC-deficient patient line WD-C1 (bottom). Primary patient cells and their isogenic gene-corrected counterparts were either untreated or treated with MMC for 48 hours and analyzed for DNA content via flow cytometry to determine functional FA correction [3,4]. Note partial correction of MMC-induced G2/M arrest in *FANCA−/−* patient cells on correction with wild-type FANCA and in *FANCC−/−* patient cells transduced with wild-type FANCC.

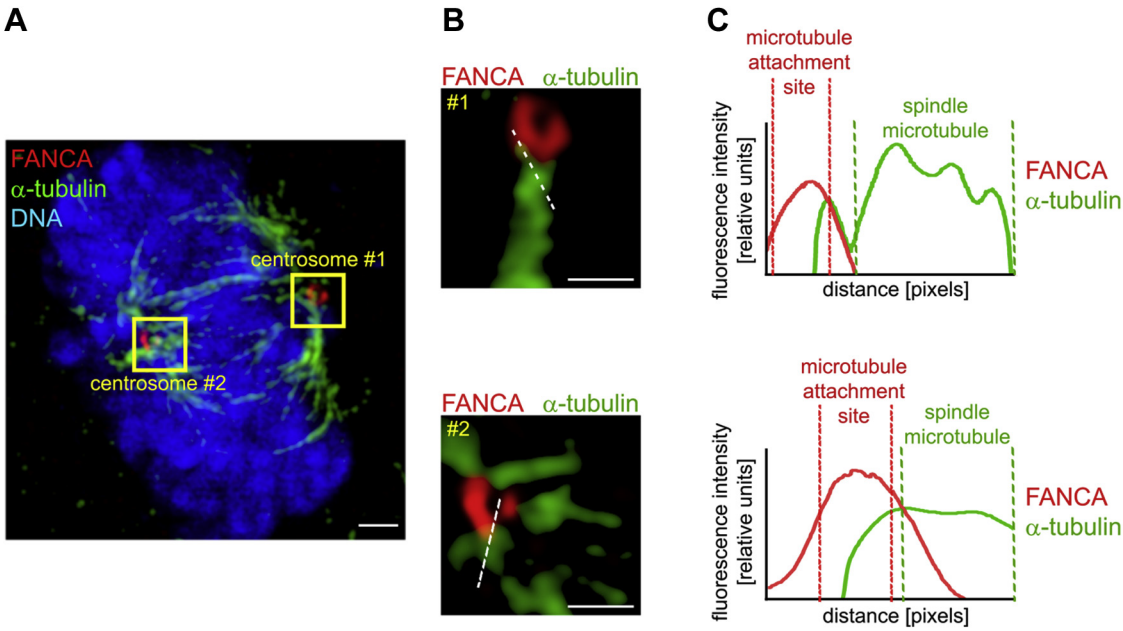

Supplementary Figure E2. FANCA localizes to the proximity of microtubule attachment sites on metaphase centrosomes. **(A)** Super-resolution image of a metaphase HeLa cell co-stained with anti-FANCA (*red*) and anti-α-tubulin (*green*) antibodies. Hoechst 33342 (*blue*) was used to counterstain DNA. Bars = 3 μm. Regions of interest marked as *yellow squares* are magnified **(B)** to show FANCA localizing to the minus end of the spindle microtubules at centrosomes. Bars = 500 nm. *Dotted white lines* indicate the FANCA and tubulin fluorescence intensity profiles provided in **(C)**.

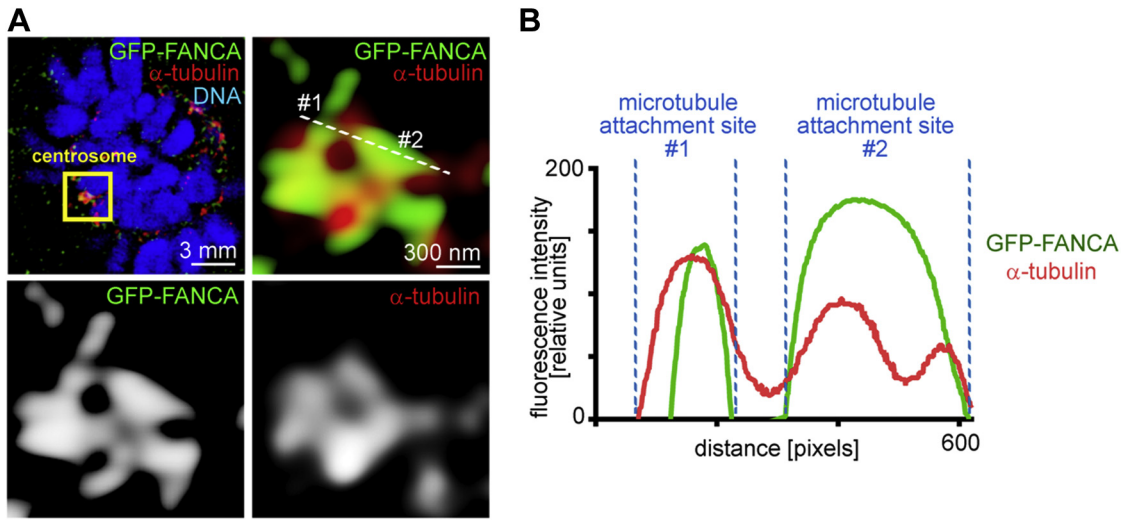

Supplementary Figure E3. FANCA-GFP is found at the minus ends of microtubules during metaphase. **(A)** Representative primary *FANCA−/−* fibroblasts stably expressing GFP-FANCA (*green*). Spindle microtubules were visualized with anti-α-tubulin antibody (*red*), and DNA was counterstained with Hoechst 33342 (*blue*). Area of interest was marked with a *yellow square*. Fluorescence intensity profile was visualized along the *white dotted line*. Bars = 3 μm (left) and 300 nm (right). **(B)** Fluorescence intensity profiles depict GFP-FANCA and α-tubulin signal peaks at two centrosome/microtubule attachment sites (#1 and #2).

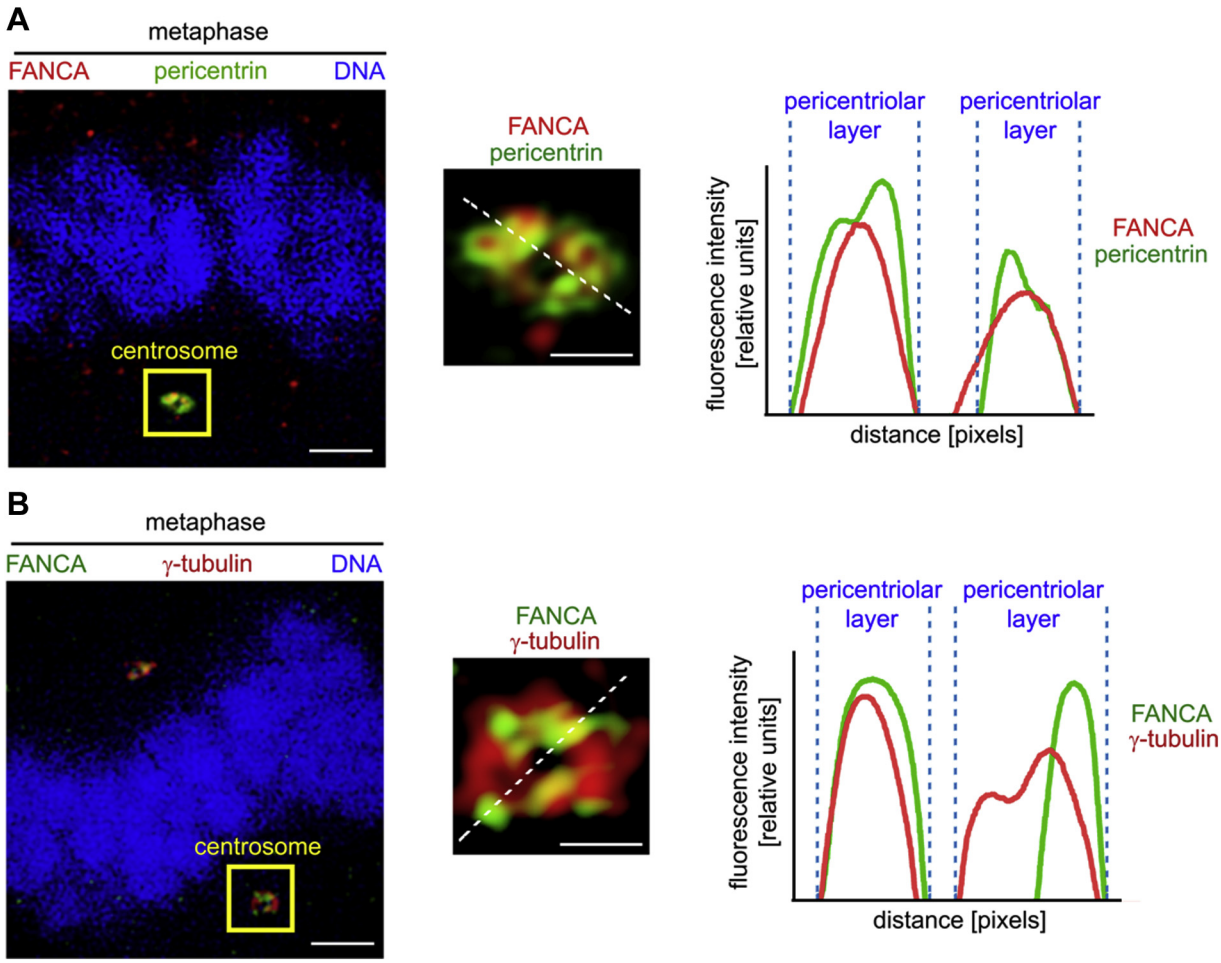

Supplementary Figure E4. Endogenous FANCA co-localizes with pericentrin and γ-tubulin during metaphase. Representative super-resolution SIM images revealing co-localization of endogenous FANCA with pericentrin **(A)** and γ-tubulin **(B)** in metaphase HeLa cells. *White dotted lines* indicate location of fluorescence intensity profiles (right). Bars = 2 μm (left) and 500 nm (right).

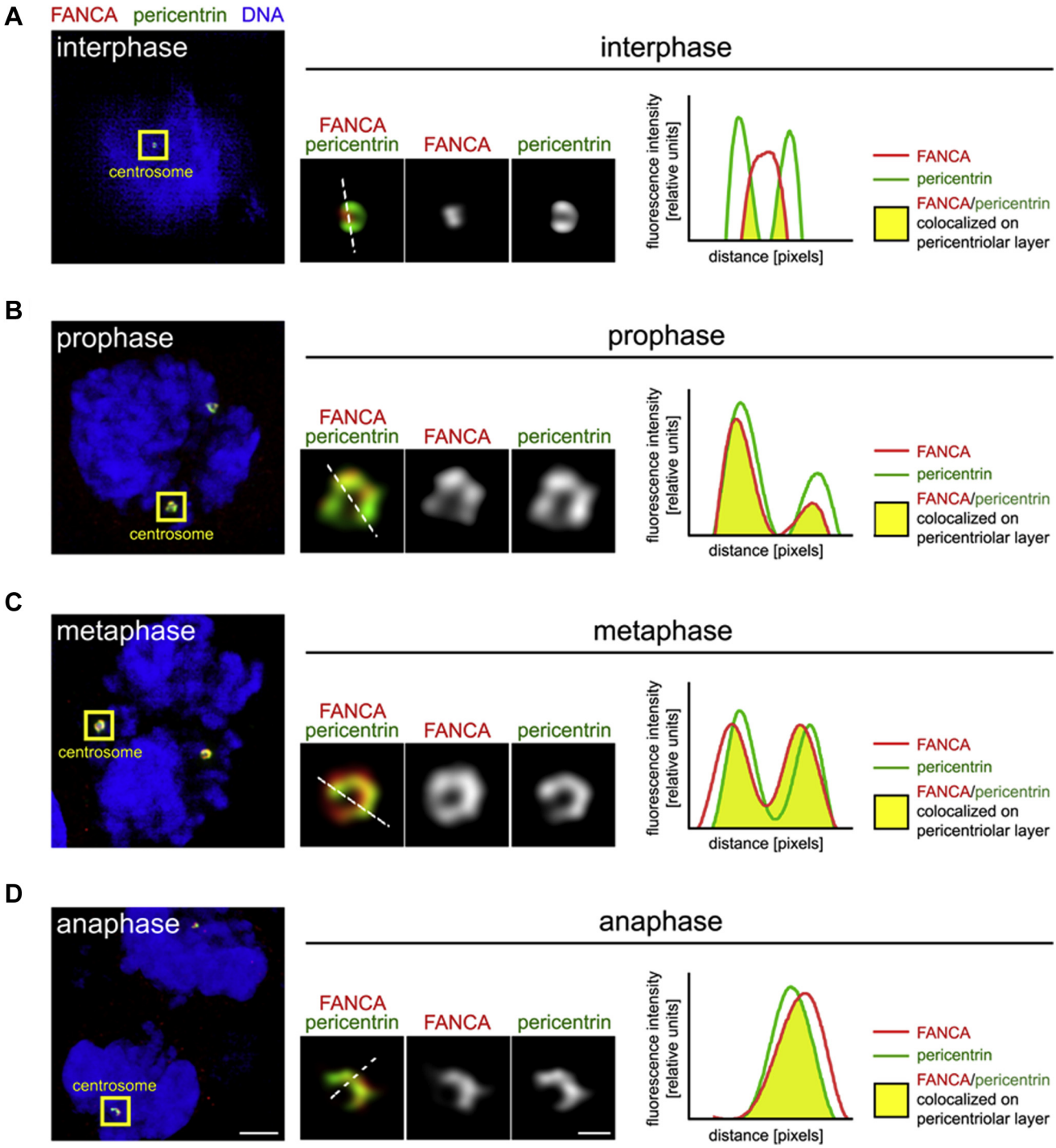

Supplementary Figure E5. FANCA and pericentrin localization profile throughout the cell cycle. SIM images of HeLa cells stained with antibodies against endogenous FANCA (*red*) and pericentrin (*green*) during interphase **(A)**, prophase **(B)**, metaphase **(C)**, and anaphase **(D)**. Centrosomes were marked with *yellow squares* and enlarged in middle panels. FANCA and pericentrin fluorescence line intensity profiles are depicted for each cell cycle stage. Note high overlap of FANCA and pericentrin peaks on mitotic centrosomes **(B–D)** compared with interphase centrosome **(A)**. Bars = 3 μm (**A–D**, left) and 500 nm (**A–D**, right).

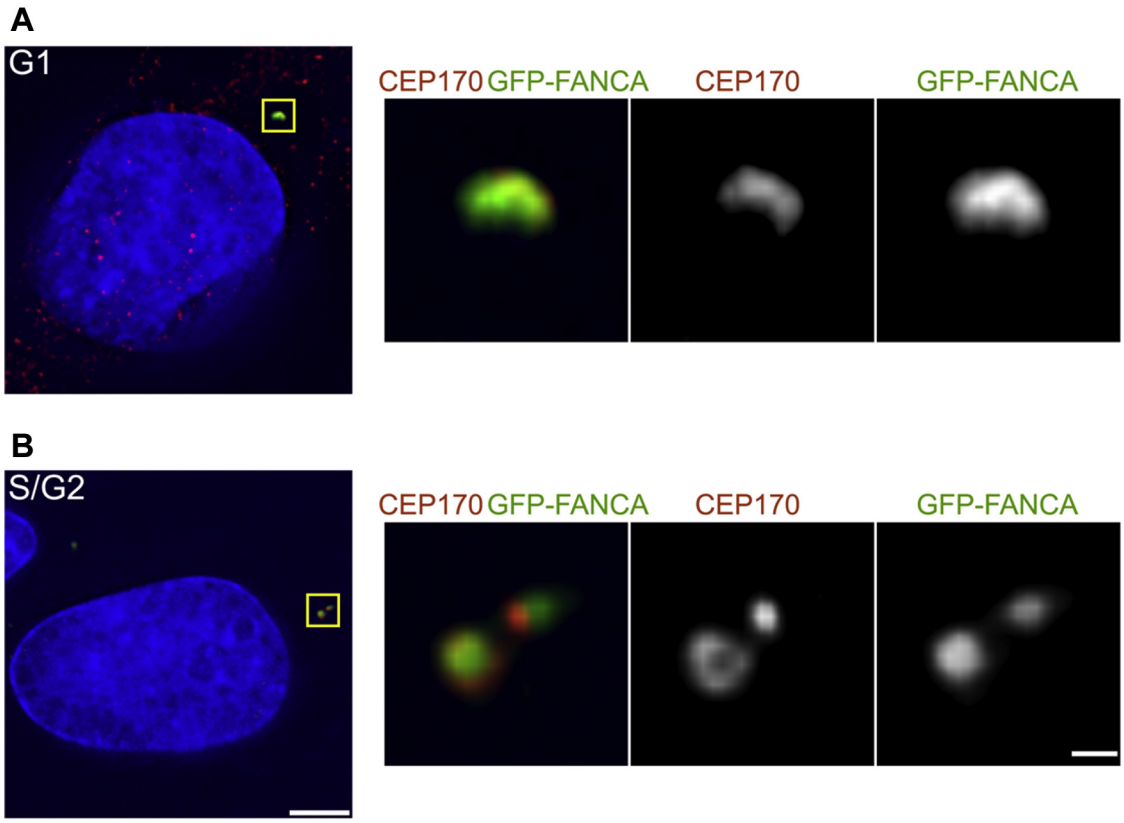

Supplementary Figure E6. FANCA localizes to the mother centriole during interphase. SIM images of primary patient *FANCA−/−* fibroblasts stably expressing FANCA-GFP stained with the antibody against the mother centriole marker CEP170 (*red*) during **(A)** G1 and **(B)** S/G2 cell cycle phases. Hoechst 33342 was used to counterstain DNA. Areas of interest marked with *yellow squares* are magnified (right panels) to show co-localization of FANCA-GFP and CEP170. Bars = 5 μm (left) and 500 nm (right).

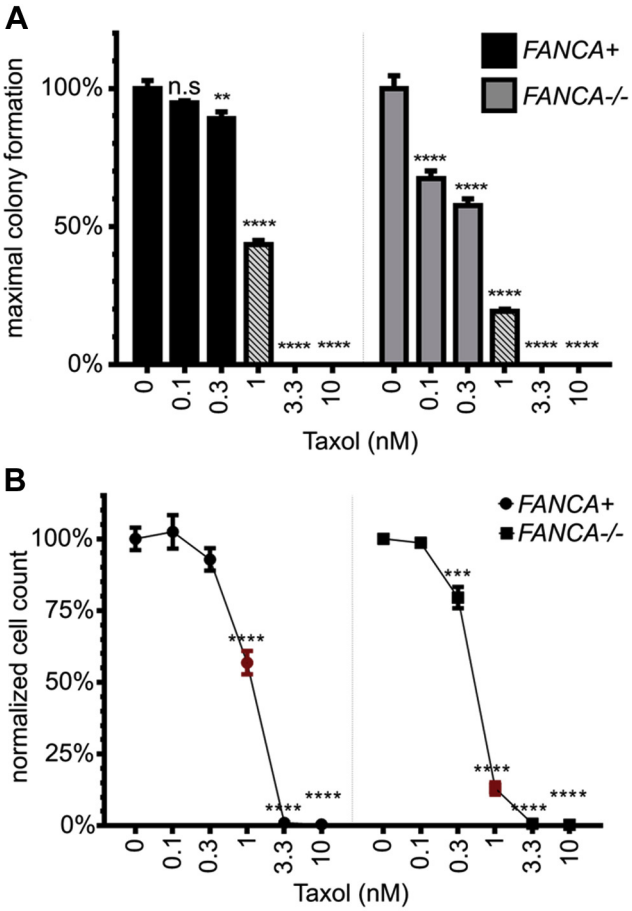

Supplementary Figure E7. Taxol dose–response curves of *FANCA*−/− and isogenic gene-corrected cells. *FANCA*−/− cells are more sensitive to taxol than *FANCA*+ cells in CFU assays **(A)** and manual cell count assays **(B)**. Two-way analysis of variance with Sidak correction was used for data analysis. Figure depicts pooled results of three separate experiments, expressed as the mean ± SEM in triplicate. *$p \leq 0.05$, **$p \leq 0.01$, ***$p \leq 0.001$, ****$p \leq 0.0001$. *ns = not significant.*

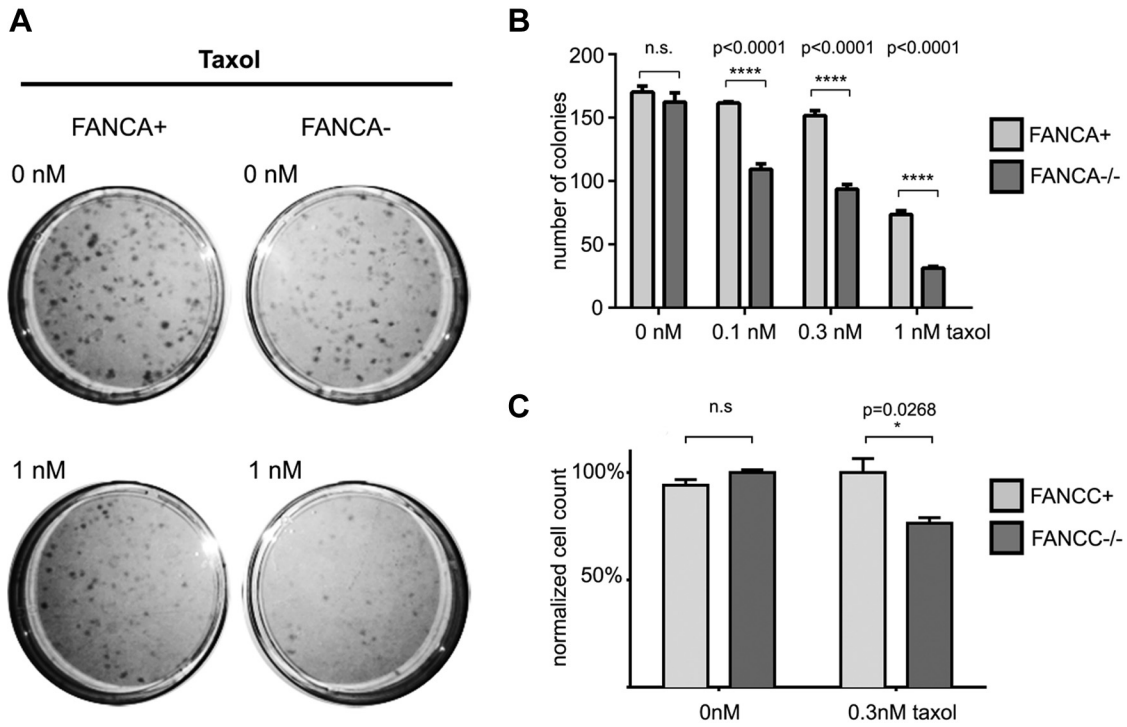

Supplementary Figure E8. Validation of taxol hypersensitivity in additional FANCA and FANCC patient fibroblast cell lines. Representative plates **(A)** and quantification **(B)** from CFU assay in which *FANCA*+ and *FANCA*−/− fibroblasts (patient line RA885) were exposed to low-dose taxol for 11 days. Error bars represent means ± SEM, and a two-way analysis of variance with Sidak correction was used to assess statistical significance. **(C)** Cell count assay of *FANCC*−/− (patient line WD-C1) cells and *FANCC*+ fibroblasts exposed to varying doses of taxol for 9 days. Statistical analysis was performed using Student's *t* test with Holm–Sidak correction.

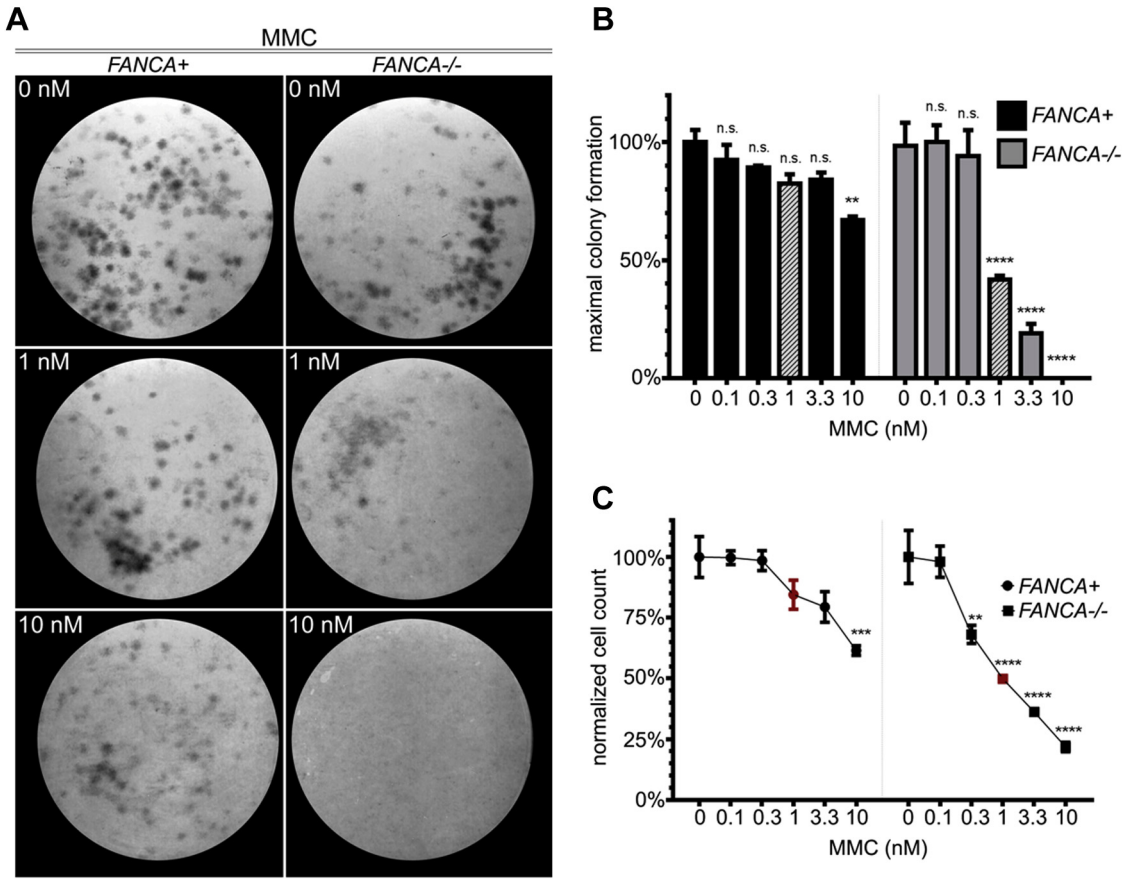

Supplementary Figure E9. Rescue of MMC hypersensitivity by FANCA gene correction in primary *FANCA−/−* patient cells. **(A)** Representative CFU assay plates of *FANCA−/−* or gene-corrected fibroblasts treated with indicated concentrations of MMC. **(B)** Normalized colony-forming ability (top) of *FANCA+* or *FANCA−/−* fibroblasts treated with indicated concentrations of MMC for 11 days. **(C)** Cell count assay (bottom) of *FANCA+* and *FANCA−/−* fibroblasts. Six-well plates were seeded with 1×10^5 cells/well and treated with indicated doses of MMC for 9 days. Cell counts were manually performed using a hemacytometer. Two-way ANOVA with Sidak correction was used for data comparison. Quantitation of data is representative of three separate experiments, and results are means ± SEM. $*p \leq 0.05$, $**p \leq 0.01$, $***p \leq 0.001$, $***p \leq 0.0001$. *ns = not significant.*

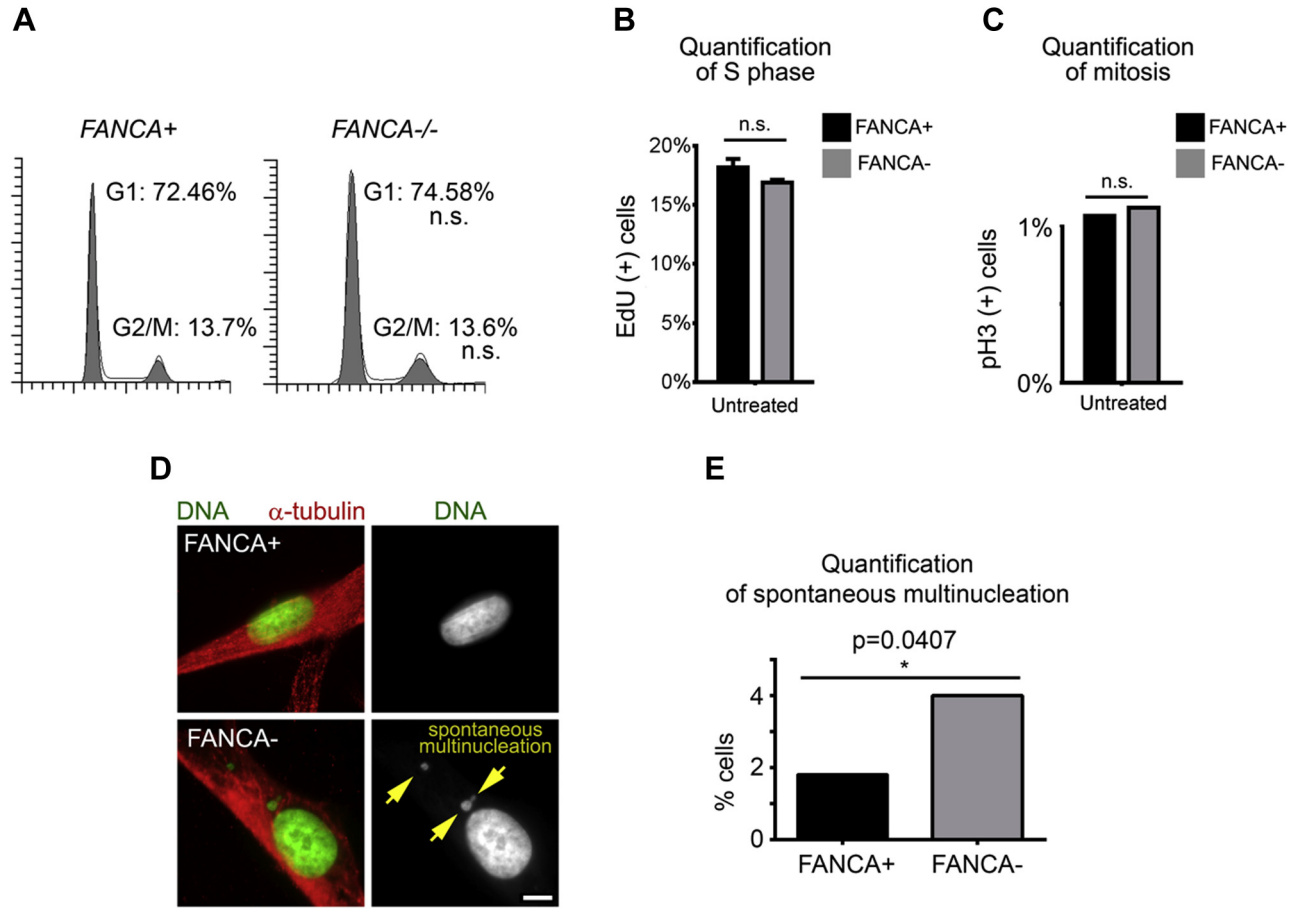

Supplementary Figure E10. Baseline cell cycle evaluation in *FANCA*−/− fibroblasts and FANCA-corrected isogenic cells. *FANCA*−/− fibroblasts do not show significant differences in G1 or G2/M cell cycle fractions quantified by PI flow cytometry **(A)**, S-phase fraction quantified by EdU incorporation via microscopy **(B)**, and phospho-H3+ mitotic fraction quantified by flow cytometry **(C)** compared with isogenic gene-corrected cells. The increase in spontaneous micronucleation **(D, E)** is consistent with previous studies [5]. Representative deconvolution microscopy images of cells of indicated genotypes are shown. Bar = 6 μm. To quantify incidence of micronucleation, at least 500 cells/genotype were imaged via deconvolution microscopy as *z* stacks spanning whole cells, and results were analyzed with Fisher's exact test. For flow cytometry analysis, data generated in three independent experiments were pooled and compared with two-tailed *t* tests. EdU incorporation counts were compared via two-way analysis of variation with Sidak's multiple comparison test.

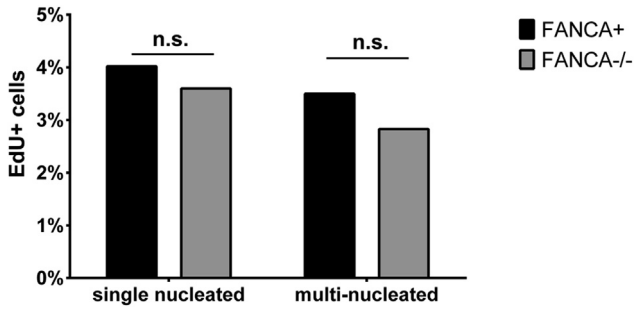

Supplementary Figure E11. Continued DNA replication in multinucleated *FANCA*−/− and gene-corrected cells. *FANCA*−/− fibroblasts and isogenic FANCA-corrected cells were treated with 1 nmol/L taxol for 9 days to induce multinucleation. Then, DNA replication in single-nucleated and multinucleated cells was quantified in EdU incorporation assays as illustrated in Figure 7. Multinucleated cells continue to replicate DNA on abnormal mitotic exit, which may promote further accumulation of DNA damage in interphase-like multinucleated cells [6,7]. The frequency of S-phase entry in multinucleated cells is not FANCA dependent ($p = 1$, Fisher's exact test; $n = 551$ FANCA−/− cells and 379 FANCA-corrected cells were analyzed).

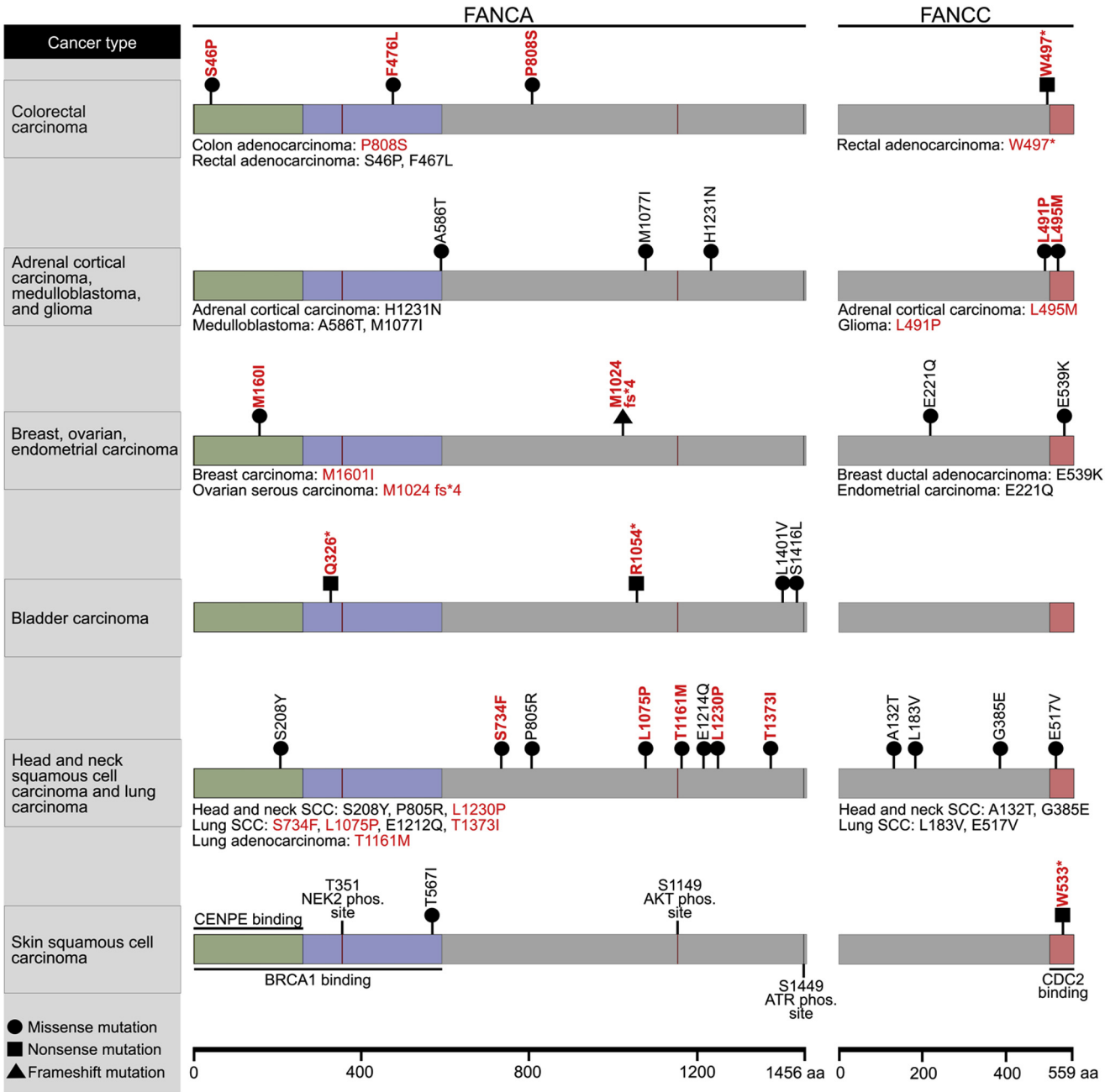

Supplementary Figure E12. Somatic mutations of *FANCA* and *FANCC* in human malignancies. Tumor samples harboring amino acid alterations resulting from confirmed missense (*circle*), nonsense (*square*), and frameshift gene mutations (*triangle*) in coding regions of *FANCA* (left) or *FANCC* (right) are shown. Mutations with predicted protein functional impact are formatted in *bold red*, whereas mutations unlikely to affect protein function are in *black*. Cancers associated with indicated mutations are on the left. Protein binding and phosphorylation sites of *FANCA* and *FANCC* are at the bottom. SCC = squamous cell carcinoma; fs*4 = frameshift that causes a translation stop four amino acids after the insertion. *Nonsense mutation.